On the function of the floccular complex of the vertebrate cerebellum: implications in paleoneuroanatomy

Sérgio Filipe Ferreira Cardoso

Dissertação para obtenção do Grau de Mestre em Paleontologia

Orientador:
Doutor Rui Alexandre Ferreira Castanhinha

Co-orientadores:
Doutor Ricardo Miguel Nóbrega Araújo
Prof. Doutor Miguel Telles Antunes

On the function of the floccular complex of the vertebrate cerebellum: implications in paleoneuroanatomy

Sérgio Filipe Ferreira Cardoso

Dissertação para obtenção do Grau de Mestre em Paleontologia

Orientador:
Doutor Rui Alexandre Ferreira Castanhinha

Co-orientadores:
Doutor Ricardo Miguel Nóbrega Araújo
Prof. Doutor Miguel Telles Antunes

Successfully defended on 18th November 2015 at FCT-UNL Campus, Portugal, before a juri presided over by:

Doutor Paulo Alexandre Rodrigues Roque Legoinha

and consisting of:

Doutor Gabriel José Gonçalves Martins

Doutor Rui Alexandre Ferreira Castanhinha

Two peer-reviewed abstracts, resulting from this study, were accepted for oral communications (Appendix II).

Ferreira-Cardoso, S., Araújo, R., Castanhinha, R., Walsh, S., Martins, R.M.S., Martins, G.G. (2014). The Floccular Complex: neuroanatomy as a tool to unveil paleoecology. Journal of Vertebrate Paleontology, Program and Abstracts, 2014, p.128.

Ferreira-Cardoso, S., Castanhinha, R., Araújo, R., Walsh, S., Martins, N.E.V., Martins, R.M.S., Martins, G.G., Kardjilov, N., Hilger, A. (2015). Floccular Complex Lobe size does not correlate with vertebrate ecology and behavior. Journal of Vertebrate Paleontology, Program and Abstracts, 2015, p.123.

The latter was awarded with a Jackson School of Geosciences Student Member Travel Grant for the 2015 Society of Vertebrate Paleontology Annual Meeting.

At the moment, this study is in submission process to Scientific Reports journal, with the following list of authors: Sérgio Ferreira Cardoso, Ricardo Araújo, Stig Walsh, Nelson E. Martins, Gabriel G. Martins, Rui M.S. Martins, Nikolay Kardjilov, André Hilger, Ingo Manke and Rui Castanhinha.

I therefore request that this document is not made available for public consultation before the publishing process is completed.

‘Look I gotta go, yeah, I'm running outta change;

There's a lot of things if I could I'd rearrange’.

Paul Hewson, David Evans, Adam Clayton & Lawrence Mullen**,** ‘The Fly’**,** *Achtung Baby*.

To all Southern Europeans who did not run out of change.

Acknowledgments

I would like to thank my mother, Ana Ferreira, and father, Sérgio Cardoso, for supporting me in this adventure that is the study of evolution. I also want to thank the rest of my family, especially my sister, Jéssica, grandfather, Duarte and grandmother, Lourdes.

I would like to thank Rui Castanhinha and Ricardo Araújo for advising, guiding and helping me to understand science, the scientific world and, above everything else, the role of a scientist in the community. Their contribution for this study, in all its components, and for my improvement as a scientist and a person was essential.

I want to thank Professor Miguel Telles Antunes for his criticism and advices.

I would like to thank Professora Ausenda Balbino for her help and support.

I also want to thank: Nelson Martins (IGC), for his help with statistics; Gabriel Martins (IGC), for his contribution to solve 3D segmentation issues; Stig Walsh (National Museums Scotland), for sharing bird data and his ideas; Nikolay Kardjilov, André Hilger and Ingo Manke (HZB), for their essential contribution with mammal data scanning; Christiane Funk, for her help and availability to give me access to Museum für Naturkunde's mammal collections.

I would like to show my gratitude to Instituto Gulbenkian de Ciência, Helmholtz Zentrum Berlin, Museum für Naturkunde, Museu da Lourinhã and Digital Morphology Museum for allowing me to use their facilities, collections or data bases.

I want to thank Fundação para a Ciência e Tecnologia (FCT) for supporting this work through the project EXPL/BIA-EVF/0665/2013 (PALEOTECH).

Finally, I want to thank Zanildo Macungo, Albano Nhassengo and Nelson Nhamutole (Museu Nacional de Geologia) for making science and for letting me be part of their science and also Issaia Macaneta and all other people involved in the PalNiassa project for building a better world.

Abstract

The cerebellum floccular complex lobes (FCLs) are housed in the FCL fossa of the periotic complex. There is experimental evidence indicating that the FCLs integrate visual and vestibular information, responsible for the vestibulo-ocular reflex, vestibulo-collic reflex, smooth pursuit and gaze holding. Thus, the behavior of extinct animals has been correlated with FCLs dimension in multiple paleoneuroanatomy studies.

Here I analyzed braincase endocasts of a representative sample of Mammalia (48 species) and Aves (59 species) rendered using tomography and image segmentation and tested statistical correlations between the floccular complex volume, ecological and behavioral traits to assess various previously formulated paleobiological speculations.

My results demonstrate: 1) there is no significant correlation between relative FCL volume and body mass; 2) there is no significant correlation between relative FCL and optic lobes size in birds; 3) average relative FCL size is larger in diurnal than in nocturnal birds but there is no statistically significant difference in mammals; 4) feeding strategies are related with different FCL size patterns in birds, but not in mammals; 5) locomotion type is not related with relative FCL size in mammals; 6) agility is not significantly correlated with FCL size in mammals.

I conclude that, despite the apparent relation between FCL size and ecology in birds, the cerebellum of tetrapods is a highly plastic structure and may be adapted to control different functions across different taxonomic levels. For example, the european mole (*Talpa europaea*) which is fossorial and practically blind, has a FCL fossae relative size larger than those of bats, which are highly maneuverable. Therefore, variation in FCL size may be better explained by a combination of multiple factors with relation to anatomical and phylogenetic evolutionary constraints.

Keywords: floccular complex, cerebellum, ecology, tomography, PGLS

Resumo

Os lobos do complexo flocular (FCLs), alojados na fossa de FCL no complexo periótico, fazem parte do cerebelo. Existem provas experimentais da integração de informação visual e vestibular pelos FCLs, sendo responsáveis pelo reflexo vestibulo-ocular, vestibulo-cólico, pela manutenção do foco visual em objectos em movimento e pela estabilização da imagem. Assim, a dimensão dos FCLs e o comportamento de animais extintos têm sido associados em vários trabalhos sobre paleoneuroanatomia.

Analisei moldes da cavidade craniana de amostras representativas de mamíferos (48 espécies) e aves (59 espécies) produzidos a partir de tomografia e segmentação de imagens. Foram testadas correlações estatísticas entre volume do complexo flocular e variáveis ecológicas/comportamentais para investigar a veracidade das especulações paleobiológicas. Os dados foram analisados com recurso regressões linearres com correcção filogenética (PGLS). Os resultados mostram que: 1) não existe correlação entre volume relativo do FCL e massa corporal; 2) não existe correlação entre tamanho relativo do FCL e os lobos ópticos das aves; 3) a dimensão relativa de FCL é maior em aves diurnas que em aves nocturnas, não havendo significância estatística para os mamíferos; 4) as estratégias alimentares estão relacionadas com diferentes padrões dimensionais de FCL em aves, mas não em mamíferos; 5) o tipo de locomoção não está relacionado com o tamanho de FCL em mamíferos; 6) a agilidade não está correlacionada com a dimensão de FCL em mamíferos.

Conclui-se que, apesar da aparente relação entre dimensão de FCL e ecologia das aves, o cerebelo é uma estrutura altamente plástica, podendo sofrer adaptações para desempenhar funções distintas em diferentes grupos taxonómicos. Por exemplo, a toupeira europeia (*Talpa europaea*), que é fossorial e praticamente cega, tem fossas de FCL relativamente maiores que os morcegos, altamente manobráveis. Sendo assim, a variação da dimensão de FCL deverá estar relacionada com factores múltiplos, sejam eles ecológicos ou relacionados com constrangimentos anatómicos e filogenéticos.

Palavras-chave: complexo flocular, cerebeloecologia, tomografia, PGLS

Index

Figures index

Table Index

Abbreviations and acronyms list

ASC – Anterior Semicircular Canal

BrainR – Brain reduced (Total Endocast Volume minus FCL)

Brainr – Brain reduced **(**Total Endocast Volume minus optic lobes)

CT – Computed Tomography

FCL – Floccular Complex Lobe

HZB – Helmholtz Zentrum Berlin, Berlin, Germany

KUPRI – Kyoto University Primate Research Institute, Kyoto, Japan

MfN – Museum für Naturkunde, Berlin, Germany

ML – Museu da Lourinhã, Lourinhã, Portugal

OL – Optic Lobes

PGLS – Phylogenetic Generalized Least-Squares

Q-Q – Quantile-Quantile

VCR – Vestibulo-collic reflex

VOR – Vestibulo-occular reflex

Introduction

The full range of sensations that allow us to feel the world, along with its consequent set of actions (behavior), is processed and determined by a combination of neuronal circuits that exist in our nervous system. A central paradigm in neuroanatomy assumes that the volume of a certain neuroanatomical structure is proportional to its functional importance. This is the principle of proper mass (Jerison, 1973). This principle refers that the evolution of intelligence is a result of increasing information processing capacity and that the latter is correlated with the amount of brain tissue (Jerison, 1973). The study here proposed exploits this general rule and highlights the complexity and integration of neuronal tissues.

A review of the anatomy, histology, development and evolutionary framework of the cerebellum

Within the central nervous system, the cerebellum is particularly interesting. It regulates movement coordination, cognition and perception (Paulin, 1993). The cerebellar cortex is composed by four main types of neurons: Purkinje cells, granule cells, Golgi cells and stellate cells (Voogd & Glickstain, 1998). The cerebellum has two major inputs (mossy fibers and climbing fibers) and one single output (composed by Purkinje cells), and appears, therefore, to be a simple circuitry (Voogd &

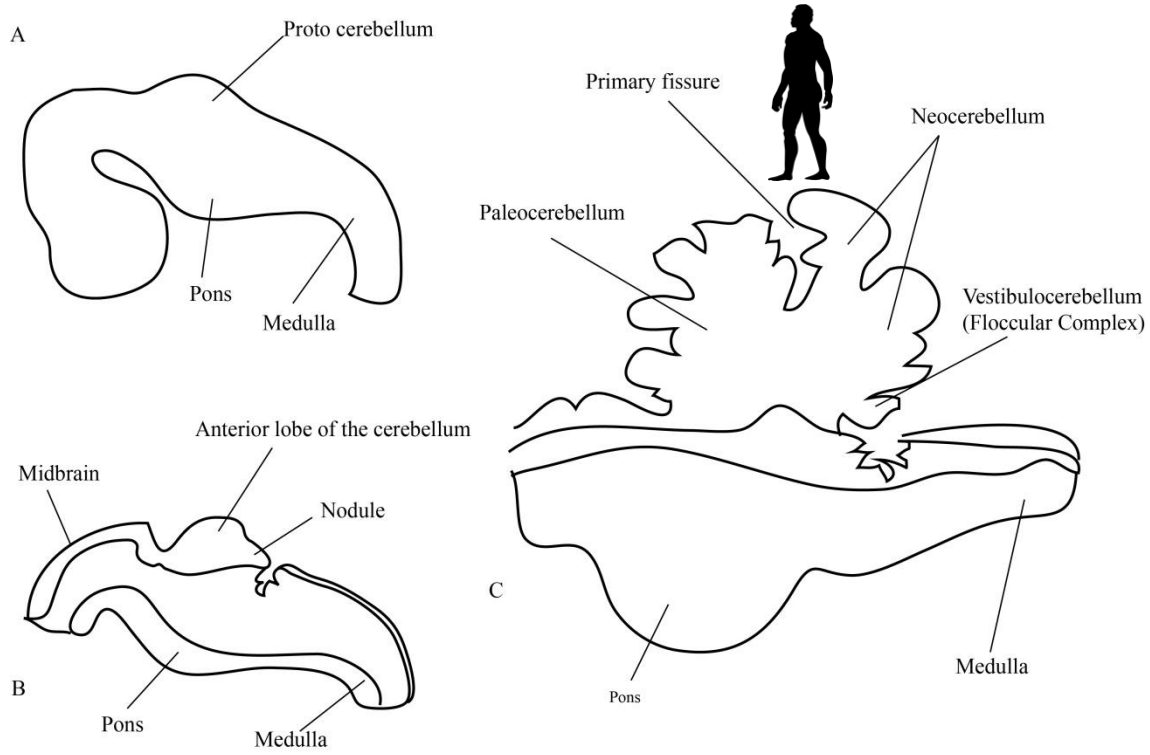

Figure 1.1 – Scheme of the development of the cerebellum, showing the early differentiation of the vestibulocerebellum of *Homo sapiens*. Brain at the end of the 5th week (A); sagittal section of the hindbrain at the age of 6 weeks (B); sagittal section of the hindbrain at the end of the 17th week. Phylopic.org silhouette – credits to T. Michaels Keesey.

Wylie, 2004). Granule cells, the most numerous cells in the cerebellar cortex, are contacted by mossy fibers via complex synapses on their dendritic terminations and their axons extend to the superficial layer of the cerebellar cortex, terminating either on dendrites of interneurons or Purkinje cells (Voogd & Glickstein, 1998). The cerebellum in hagfishes and lampreys is simply a group of modified cells of the acusticolateral area of the medulla oblongata (Johnston, 1901 in Larsell, 1967). In urodeles, the cerebellar structure is similar to those of hagfishes and lampreys but the corpus cerebelli, which receives proprioceptive and other sensory impulses, becomes more developed and eventually the predominant feature of the cerebella of selachians, teleosts and all amniotes (Larsell, 1967).

Table 1.1 – General divisions of the cerebella of mammals and birds according to Ziehen (1899)

Vermis lobules	**Hemispheral lobules**	**Folia**
Lingula	Vinculum lingulae	I
Lobulus centralis	Ala lobuli centralis	II & III
Culmen	Lobulus quadrangularis (Pars anterior)	IV & V
Declive	Lobulus quadrangularis (Pars posterior)	VI
Folium vermis	Lobulus semilunaris superior	VII A
Tuber vermis	Lobulus semilunaris inferior	VII B
Pyramis	Lobulus biventer	VIII
Uvula	Tonsilla (dorsal paraflocculus)	IX
Nodulus	Flocculus/ventral paraflocculus	X

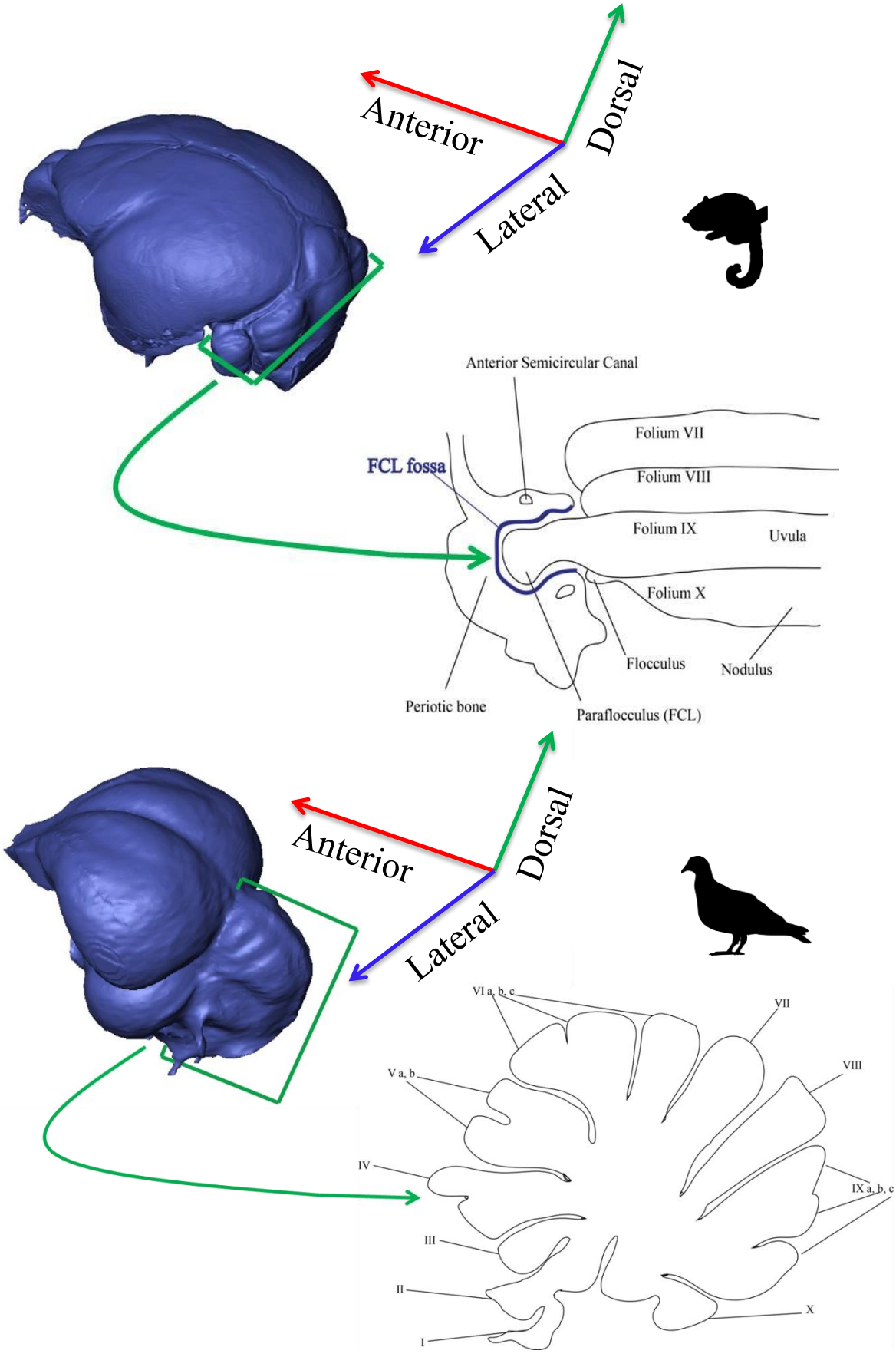

Figure 1.2 – Schematic illustration of a *Microcebus murinus* floccular complex with bones of the periotic complex transversally cut (dorsal view) (above); schematic illustration (parasagittal section) of an *adult Columba livia* cerebellum (adapted from Larsell, 1967) with identification of the 10 folia listed on table 1.1 (below). Phylopic.org silhouettes – creditis to Maky, Skollar & Lewis and Viatour & Plank.

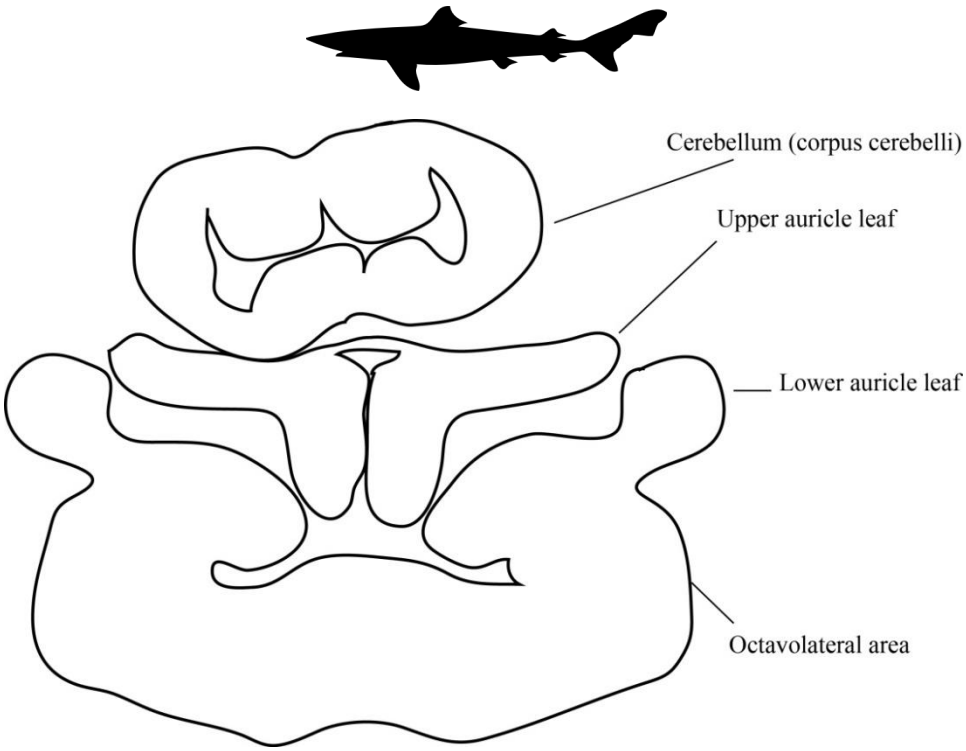

Figure 1.3 – Schematic illustration of a coronal section of a cerebellum of a *Scyliorhinus canicula* (Adapted from Pose Mendez (2013)). It is possible to see the auricle, which corresponds to the FCL, and the immediately adjacent octavorateral area, which functions are related with to detection of vibrational signals by the octavolateral system (which comprises the ear and the mechanosensory lateral line). Phylopic.org silhouette uncredited.

During development, the ectodermal plate (Figure 1.1) begins folding dorsally, which originates the formation of the neural tube. The closure of the rostral neuropore originates the three primary brain vesicles: the prosencephalon (forebrain), the mesencephalon (midbrain) and the rhombencephalon (hindbrain) (Gilbert, 2010; Shekdar, 2011). Neural tube bending develops two flexures - cephalic and cervical – and later a new dorsal flexure is developed in the middle of the former two – the pontine flexure – thus dividing the rhombencephalon in two portions, the metencephalon and the myelencephalon (Gilbert, 2010; Shekdar, 2011). The cerebellum originates from both the rostral portion of the metencephalon and the caudal portion of the mesencephalon (Hallonet et al., 1990; Christensson, 2007; Fotos et al., 2011). It can be divided into three parts: the vestibulocerebellum (or archicerebellum), which is the phylogenetically oldest part of the cerebellum and has connections with the vestibular apparatus; the paleocerebellum, which is phylogenetically more recent than the vestibulocerebellum and is related to density data from limbs; the neocerebellum, which controls limb movements and is the part of the cerebellum that appeared more recently in the evolution of the brain (Voogd & Glickstain, 1998; Shekdar, 2011). The cerebellum is a folded structure typically divided in folia (Larsell, 1967; Voodg & Glickstein, 1998). The nomenclature here used is presented in table 1.1 (see Figure 1.2). This work will focus on the vestibulocerebellum, which

includes the flocculus, paraflocculus, nodulus and uvula, or simply: the floccular complex (Figures 1.2) that correspond to folia IX and X of Ziehen (1899) nomenclature (Larsell, 1967; Voogd & Glickstain, 1998; Kheradmand & Zee, 2011). It is difficult to establish homologies between specific folia in phylogenetically distant taxa but the basic functions of the floccular complex are common to all cerebella. This happens because the basic cerebellar divisions in all gnathostomes consists of auricles (which corresponds to the FCLs) and cerebellar body (Larsell, 1967; Paulin, 1993; Pose Mendez, 2013). According to Pose Mendez (2013), the upper and lower auricle leaves of the cerebellum of cartilaginous fishes are homologous to the vestibulocerebellum. Studies suggest that the upper auricle leaf (Figure 1.3) is homologous to the X folium of the amniote cerebellum, which corresponds to the flocculus and nodulus (Pose Mendez, 2013). In general, the *eminentia granularis* (a part of the vestibulolateral lobe of fish and amphibians cerebella that is the location of some nerve synapsis of the lateral line) performs functions related to vestibular and proprioceptive perceptions in fishes and even in anurans. Nevertheless, it is the *torus longitudinalis* (granular cells that develop in the cerebellum of teleost fishes) that is presumed to control posture, detect luminance levels and monitor saccadic movements in teleosts (Kotrschal et al., 1998; Albert, 2001). Larsell (1967) refers that the modified *eminentia granularis* of anurans is homologous to flocculi of birds and mammals.

The floccular complex of the cerebellum

The floccular complex of the cerebellum is a center for integration of visual and vestibular stimuli while controlling the extraocular muscles (Zee et al., 1981; Voogd & Wilie, 2004). There is a connection between the axes of the three semicircular canals, the three extraocular muscles and the rotation axes of the field of view, because floccular zones project to extraocular motorneurons, via cerebellar nuclei, which causes eye rotation according to the best response axis of the climbing fibers (De Zeeuw et al., 1994 *in* Wylie et al, 1994). The compartmentalization of the flocculus reflects the monitoring of eye rotation, because each compartment projects to two of the extraocular muscles (Winship & Wylie, 2003).

Several studies have focused on the retina image stabilization function (Ito, 1982; Nagao, 1992; Nagao et al, 1997; Winship & Wylie, 2003). The vestibulocerebellum's floccular complex is involved in posture, balance and head/eye movements control (Paulin, 1993; Netter et al., 2002). In mammals and birds, the vestibulocerebellum is composed by the: flocculus, paraflocculus, nodulus and ventral uvula (Larsell, 1967; Ito, 1982; Angelaki & Hess, 1994). The floccular complex regulates compensatory movement of the eyes to respond to rotational movements of the head (vestibulo-ocular reflex, VOR), or to track a moving object in the field of view (smooth pursuit) and also contributes to stabilize the head via cervical muscles (vestibule-collic reflex, VCR) (Ito, 1982; Waspe et al., 1983; Burdess, 1996; Voogd & Wylie, 2004). The flocculus/paraflocculus responds to brief vestibular stimuli, sustaining pursuit eye movements and gaze holding, while the nodulus/ventral uvula act during sustained vestibular responses (Kheradmand & Zee, 2011). VOR processing can adapt and

learning allows the reduction of error in rapid responses during flight speed alterations, acrobatic maneuvers in aquatic environments or prey tracking during high-speed pursuit predation (Ito, 1998; Witmer et al., 2003, Walsh et al., 2013). A signal is transferred from mossy fibers afferents to Purkinje cells and this signal can be "corrected" because of a unique dual input system existing in the cerebellum (Ito, 1982). Given the retinal errors, neuronal networks of the floccular complex may be reorganized by the visual climbing fiber afferents, resulting in improvement and adaptation of the VOR (Ito, 1982).

The present work focuses on the lateral projections of the cerebellum that comprise the flocculus and paraflocculus. Several terminologies have been used to refer both to the FCL and the fossa housing it, flocculus, paraflocculus, cerebellar auricula, *fovea floccularis* (Olson, 1944; Larsell, 1967; Hopson, 1979; Gannon et al., 1988; Ivakhnenko, 2008; Castanhinha et al., 2013). For simplicity and correction, and because I used bird and mammal endocasts, I will hereinafter refer to these lateral projections as floccular complex lobes (FCLs).

The FCLs protrude into the periotic and prootic bones (in mammals and birds, respectively) and are housed in the FCL fossa (Figure 1.2). FCL fossae are present in distinct groups of animals such as: dinosaurs (birds, non-avian theropods, ornithopods, sauropods) (Franzosa, 2004; Miyashita et al, 2011; Walsh et al., 2013; Thomas, 2015) pterosaurs (Witmer et al., 2003) mammal-like reptiles (Olson, 1944; Castanhinha et al., 2013; Laaß , 2015) and mammals (Olson, 1944; Gannon, 1988) (Figure 1.4). I assume that the FCL fossa volume is a good proxy to access the FCL volume as it is assumed that bird and mammal endocasts are good aproximations of brain morphology and size (Jerison, 1973; Hopson, 1979; Gannon, 1988; Iwaniuk & Nelson, 2002; Macrini et al., 2007). In fact, Edinger (1948 *in* Lyras, 2009) comments that the study of brain external morphology with endocasts provides, in most mammals, more reliable information than real brains.

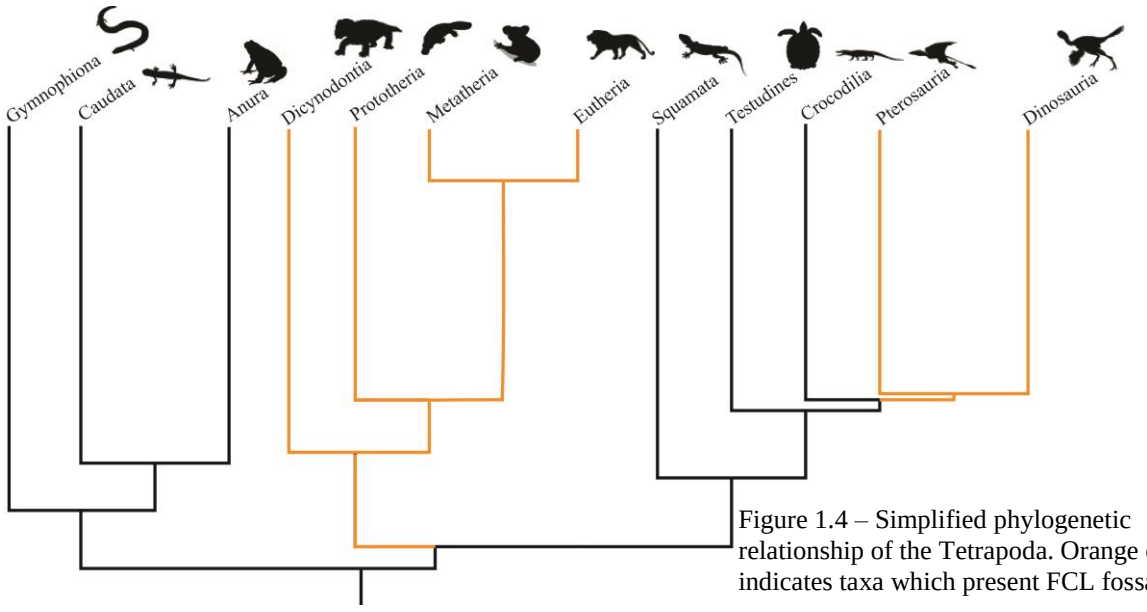

Figure 1.4 – Simplified phylogenetic relationship of the Tetrapoda. Orange color indicates taxa which present FCL fossae.

Paleobiological speculations on the floccular complex function

There are several examples in the literature of direct or indirect association between FCL fossae size and high maneuverability and agility in birds (Milner & Walsh, 2009; Walsh & Milner, 2011), dinosaurs (Domínguez et al., 2004, Franzosa, 2004), and pterosaurs (Witmer et al., 2003). Therapsid large FCL fossae casts have also been associated to an active life style (Olson, 1944; Laaß, 2015), as well as to locomotion in three-dimensional environments such as aquatic environments (Ivakhnennko, 2008). In addition, Gannon (1988) noted a correlation between the increase of FCL fossae relative size and the decrease of body mass in mammals.

There are, however, some issues about the FCL function that may blur the analysis of the FCL size variation, namely the plasticity of the cerebellum and its unclear functional compartmentalization. Although FCLs are functionally related to eye movement and image stabilization, eye motor control is not exclusively performed by these lobes, but also by the ventral uvula, nodulus or oculomotor vermis, for example (Rambold et al., 2002; Kheradman & Zee, 2011).

Nevertheless, some interesting speculations have been proposed about the FCL and ecology. Franzosa (2004) observed that theropod dinosaur brain specimens tended to decrease in size and therefore body mass and suggested that during theropod evolution there was an enlargement of the optic lobes and cerebral hemispheres. Franzosa (2004) also suggested that as optic lobes increase, FCLs also increased in size. This would be explained by the fact that theropods became active predators (instead of scavengers) and a decrease in prey size demanded more speed and agility from the predator (Hopson, 1980). Increased optic lobes, cerebral hemispheres and FCLs size indicates that there was a selective pressure for improved agility and hand-eye coordination in theropods (Russel, 1969; Pearson, 1972). The conspicuity of the FCLs has also been related to the acquisition of flight capacity (Domínguez et al., 2004) which, once again, relates agility/maneuverability and the relative size of these structures.

Other than eye motor control functions were suggested by Witmer et al. (2003) for pterosaurs. It was hypothesized that the large FCLs of *Rhamphorhynchus muesteri* and *Anhanguera santanae* were related to processing of proprioceptive and somatosensory information produced by the membranous wings (Witmer et al., 2003). This suggestion was based on Winship & Wylie (2003) study. However, evidence to support such speculation is not clear. In primates, Gannon (1988) noted a negative correlation between body mass and FCL relative size. Great apes (e.g., *Homo sapiens*) lose the FCL fossa after birth, only remaining a smaller accessory paraflocculus (Spoor & Leakey, 1996). Probably, large FCLs are plesiomorphic to extant mammals (Kielen-Jaworowska, 1986). Olson (1944) briefly discusses variation in FCL fossa depth and refers that smaller and very active animals have large FCLs and tend to have large periotic bones. This could represent that the FCLs size is conditioned by a more complex set of morphological constraints. Paulin (1993) argues that FCLs function in bats may be associated with echolocation instead of eye movement control. The idea that

FCLs have other functions besides eye motor control (Paulin, 1993; Witmer et al., 2003) are supported by the cerebellum evolutionary history (Larsell, 1967) and its plasticity, and will be discussed later on.

Testing paleobiological speculations

I will use CT-scanned braincase endocasts (Balanoff et al., 2015) of extinct and extant species to test the relation between the relative volumes of the FCL fossa under the following hypotheses:

Hypothesis I, larger animals present proportionally smaller FCL. Rationale: the amount of neural tissue required to process a certain neural input might have a limit so in animals with bigger brains the quantity of neurons present in the a large cerebellum might be enough to process all the required inputs without the need of producing a larger FCL fossa (Gannon, 1988; Franzosa, 2004);

Hypothesis II, slower animals have smaller FCL fossae; Rationale: animals with more agility should need a larger amount of neural tissue to process visual and vestibular stimuli to improve image stabilization accuracy (Olson, 1944; Franzosa, 2004);

Hypothesis III, different locomotion strategies correspond to different FCL size patterns; Rationale: similar to Hypothesis II with a different categorization;

Hypothesis IV, feeding habits can be correlated with FCL size. Rationale: niches which primarily require an optimized vision should be occupied by animals with efficient eye movements (Hopson, 1980);

Hypothesis V, size of FCL and optic lobes of birds are positively correlated. Rationale: increased FCL fossa volumes suggest a better vision acuity and are possibly associated with enlargement of the optic lobes in vision-dependent animals (Franzosa, 2004);

Hypothesis VI, animals with different circadian activity patterns present different FCL sizes. Rationale: given the different level of reliance in vision of diurnal and nocturnal animals, there is a difference between FCL relative sizes in these two groups.

Hypothesis VII, size of FCL and area and perimeter of the anterior semicircular canal (ASC) are positively correlated. Rationale: since the FCLs are constricted by the ASC, it is expected that larger relative ASC areas and perimeters correspond to larger relative FCLs.

I will here discuss, basing on the results for each hypothesis, the reported assumptions that FCL fossa volume can shed light on animal ecology.

Material and Methods

Important concepts of statistical analyses

This section aims to facilitate the interpretation of the Materials and Methods section. The topics/concepts are ordered according to the order of appearance on the text.

Logarithmic base-10 transformation – Parametric statistical tests require data or residuals to be normally distributed, thus the original data may need to be transformed to meet such assumptions. Therefore, it is possible to perform a mathematical operation to transform data, thus it may fit a parametric statistical test, such as an Anova or a linear regression (McDonald, 2014). Many biological variables have log-normal distribution, which means that data is normal after a logarithmic transformation (McDonald, 2014). Logarithmic transformations are commonly used to transform size data and, by using a Log 10 transformation it is easy to see the magnitude of the original number (e.g., log(10)=1, log(100)=2, etc.) (Spoor et al., 2007; Walsh et al., 2013; McDonald, 2014). I here used base-10 log transformation to normalize data.

Linear regression / Residuals – When a linear regression is computed, each of the observed values of the predictor (x) and response (y) variables create a line showing a trend of the values along the x and y axes. This line is given by $y=mx+b$, where m is the estimated slope and b is the estimated intercept (value of y when $x=0$) (Verzani, 2014). To each data point there is a corresponding estimation, which is a point of the estimated regression line (Verzani, 2014). The difference between the response variable observed value and the predicted value (given by the interception of the regression line and the corresponding predictor value) is called a residual (Verzani, 2014). Geometrically, a residual is the vertical distance of a given point (x_i,y_i) to the regression line.

Generalized Least-squares – GLS is a technique to estimate unknown parameters of a linear regression model. When a regression line is produced in a graph, it minimizes the squared vertical distances between the data points and the line (Greene, 2003; McDonald, 2014). To each x_i of a data point corresponds a y_i and an estimation,$\hat{y}$. The difference between y_i and $\hat{y}$ is calculated and squared and the sum of the squared deviates of all data points is a measure of how well the regression line fits the data (Greene, 2003; McDonald, 2014). Among the pool of possible lines to fit the data, the regression line is the chosen one with the smallest sum of squared deviates. It may happen that errors (or disturbances) have a non-constant variance (heterokedastic) or are correlated (autocorrelation) and in that case a Generelized Least-squares estimator can be used, converting a heterokedastic into a homokedastic model (Greene, 2003). For further reading on the theory of Generalized Least-squares estimation see chapter 10 of *Econometric Analysis* that deals with the detailed mathematics details involved in this process (Greene, 2003).

Prediction interval – In regression analysis there are two types of interval usually referred: confidence intervals and prediction intervals. Confidence intervals are related with estimation of parameters and contain all the null hypotheses that would not be rejected given a α% significance level

(Faraway, 2002). In practice, confidence intervals are related with the regression line and contain the parameter values that should not be rejected.

A prediction interval gives an estimate of a range of values where future observations will fall, taking into account the analyzed sample, with a confidence of 100(1-α)% (Garland and Ives, 2000). In this case, instead of a parametric distribution, the intervals predict the distribution of individual future points. On both cases there are two limits, the upper and the lower, which are frequently represented in regression plots (e.g., Figure 2.6).

Collinearity – Collinearity or multicollinearity among predictors (independent variables) is not desirable (Mundry, 2014). When two predictors, or a group of more than two, are strongly correlated, they provide the same information, which means they are redundant variables (Mundry, 2014). Collinearity has two main consequences: 1) conclusions about collinear predictors are unreliable, with increased standard errors of parameter estimates and unreliable non-significance ($P > 0.05$) being the main problems; 2) a model with collinearity is unstable and results can be altered by small changes (Mundry, 2014). To address this, the inspection of variance inflation factors and consequent drop of the problematic variable(s) is advisable (Mundry, 2014).

Covariance matrix – A covariance matrix (or variance-covariance matrix) is a theoretical matrix derived from a phylogenetic tree which quantifies species divergence from their common ancestor (variance) and resemblance among species (covariance) (Paradis, 2011). A matrix of this type is therefore essential to perform Phylogenetic Generalized Least-squares analysis, thus improving the linear model.

Ultrametric tree – Phylogenetic trees have branches which represent some kind of distance between species. These branch lengths have variable distance types, depending on data type and resources available to build a tree. An ultrametric phylogenetic tree is the one in which all tips (species) are equally distant from the common ancestor.

Micro-CT scans

A total of 47 extant mammal species and 1 Anomodontia species were selected to cover the widest ecological range possible (see Table 2.1). From these, I scanned 27 skulls from the mammal collections of the Museum für Naturkunde (MfN) at the micro-CT in Helmholtz Zentrum Berlin (HZB) (see Figure 2.1). The selected skulls were placed into cylindrical plastic containers and accommodated with pieces of styrofoam, both to protect the specimen's fragile structures and avoid displacement from the original position (see Figure 2.2). X-ray µCT scanning was performed with a micro-focus 150 keV Hamamatsu X-ray source with a tungsten target and a flat panel detector C7942 (120x120 mm, 2240×2368 pixel, pixel size 50 µm). All the specimens were scanned with an acceleration voltage of 100 keV and a beam current of 95 µA with an exposure time of 0,5 seconds. Image noise was reduced by using a 3-fold integration. The source-object distance was 220 mm and a source-detector distance of 300 mm was used, thus achieving a magnification factor of 1.36. The number of acquired projections varied between 800 and 1000. In the X-ray cabinet the sample was rotated in a precision rotation stage from Huber, Germany. I used Octupus V8.6 software to implement the back-projection algorithm with convolution and correction for cone beam. The average voxel size of the reconstructed volumes was 36,8 µm. The resulting data sets were binned (2x2x2, average binned) using software FIJI (Schindelin et al., 2012). This process performs an eight-fold reduction of data size to facilitate processing and handling.

Figure 2.1 – Micro-CT setup at the HZB.

Figure 2.2 – Cylindrical plastic containers pilled and glued, with specimens inside.

Table 2.1 – List of mammal and anomodont species used in this study and their meausured FCL fossae volume, braincase endocast volume, and FCL % of the endocast. Volumes result from the sum of both left and right FCLs. Species are ordered and phylogenetically grouped.

Species	Common name	FCL volume (mm^3)	Endocast volume (mm^3)	FCL %
Ornithorhynchus anatinus	Platypus	56,63	9732,84	0,58
Cebus apella	Tufted capuchin	252,58	68123,24	0,37
Brachyteles arachnoides	Southern muriqui	232,07	110426,26	0,21
Lagothrix lagotricha	Humboldt's woolly monkey	561,00	95153,29	0,59
Alouatta caraya	Black Howler	257,75	48899,50	0,53
Hylobates agilis	Agile gibbon	90,56	105684,25	0,09
Otolemur crassicaudatus	Brown greater galago	50,05	9926,55	0,50
Presbytis melalophus	Sumatran surili	130,58	73154,19	0,18
Microcebus murinus	Grey mouse lemur	25,13	1549,58	1,62
Varecia variegata	Black-and-white ruffed lemur	328,99	32013,42	1,03
Propithecus verreauxi	Verreaux's sifaka	199,94	23437,61	0,85
Lepus capensis	Cape hare	263,81	12106,82	2,18
Idiurus macrotis	Long-eared Flying Mouse	10,42	836,64	1,25
Anomalurus derbianus	Lord Derby's scaly-tailed squirrel	116,95	6655,76	1,76
Ondatra zibethicus	Muskrat	39,59	4524,33	0,88
Arvicola terrestris	European water vole	8,73	1124,55	0,78
Mus musculus	House mouse	3,81	390,18	0,98
Rattus norvegicus	Brown rat	15,86	1904,64	0,83
Dipodomys deserti	Desert kangaroo rat	18,50	1766,76	1,05
Marmota marmota	Alpine marmot	145,96	11615,83	1,26
Sciurus vulgaris	Red squirrel	126,64	6151,98	2,06
Ratufa bicolor	Black giant squirrel	203,25	12005,61	1,69
Ratufa affinis	Cream-coloured giant squirrel	206,51	9686,79	2,13
Talpa europaea	European mole	26,47	1133,21	2,34

Vulpes vulpes	Red fox	19,65	50355,69	0,04
Ursus americanus	American black bear	296,54	238402,84	0,12
Lutra lutra	European otter	84,43	44655,21	0,19
Meles meles	European badger	133,27	40130,94	0,33
Paradoxurus sp.	Palm civet	13,71	20450,59	0,07
Prionailurus iriomotensis	Iriomote cat	18,24	34932,50	0,05
Felis catus	Domestic cat	8,31	27506,92	0,03
Puma concolor	Cougar	23,07	187732,02	0,01
Rousettus aegyptiacus	Egyptian fruit bat	25,64	2221,33	1,15
Pteropus giganteus	Indian flying fox	33,48	8963,99	0,37
Rhinolophus ferrumequinum	Greater horseshoe bat	6,21	351,52	1,77
Diphylla ecaudata	Hairy-legged vampire bat	13,63	690,72	1,97
Desmodus rotundus	Common vampire bat	16,40	910,69	1,80
Molossus rufus	Black mastiff bat	7,61	437,80	1,74
Procavia capensis	Rock hyrax	7,23	13980,43	0,05
Potamogale velox	Giant otter shrew	22,20	3968,67	0,56
Oryzorictes sp.	Rice tenrec	11,10	521,63	2,13
Dasyurus hallucatus	Northern quoll	45,51	3339,75	1,36
Petaurus sp.	Flying phalanger	46,38	3444,60	1,35
Phascolarctos cinereus	Koala	110,78	26275,29	0,42
Dromiciops gliroides	Monito del monte	11,87	821,00	1,45
Monodelphis domestica	Gray short-tailed opossum	11,34	956,06	1,19
Didelphis virginiana	North American opossum	39,17	6608,01	0,59
Niassodon mfumukasi **(ML ML1620**	-	20,00	1082,00	1,85

Table 2.2 – List of bird species used in this study and their meausured FCL volume, braincase endocast volume, and FCL % of the endocast. Volumes result from the sum of both left and right FCLs and OLs. Endocast and FCL volumes from Walsh et al. (2013). Species are ordered and phylogenetically grouped.

Species	**Common name**	**FCL volume (mm^3)**	**Endocast volume (mm^3)**	**Optic lobes volume (mm^3)**	**FCL %**
Rhynchotus ruficens	Red winged tinamou	14,86	3690,58	439,92	0,40
Apteryx haastii	Great spotted kiwi	32,24	12496,13	88,72	0,26
Dromaius novaehollandiae	Emu	236,13	27054,5	2002,03	0,87
Casuarius casuarius	Cassowary	271,95	32724,27	2274,34	0,83
Struthio camelus	Ostrich	195,92	36517,99	2585,47	0,54
Rhea americana	Greater rea	153,76	13713,05	1364,45	1,12
Phasianus colchicus	Common pheasant	29,78	4021,23	530,80	0,74
Gallus gallus	Red junglefowl	35,87	3976,07	452,87	0,90
Cygnus olor	Mute swan	149,53	17360,36	447,90	0,86
Aythya fuligula	Tufted duck	38,97	5351	277,72	0,73
Tachyeres brachypterus	Falkland steamer duck	92,15	6667,4	288,03	1,38
Phaethon lepturus	White tailed tropic bird	40,5	2803,58	408,48	1,44
Opisthocomus hoazin	Hoatzin	33,33	3370	194,79	0,99
Podiceps cristatus	Great crested grebe	44,61	3303,11	334,27	1,35
Gavia immer	Great northern loon	179,58	12284,93	829,23	1,46
Pelagodroma marina	White faced storm petrel	3,92	496,91	51,28	0,79

Diomedea exulans	Wandering albatross	192,4	29151,6	760,86	0,66
Pelecanoides urinatrix	Common diving petrel	64,3	1351,72	90,29	4,76
Fulmarus glacialis	Northern fulmar	48,96	7440,16	174,10	0,66
Eudyptula sp.	Little penguin	64,3	8522,17	557,35	0,75
Ciconia ciconia	White stork	56,15	11348,13	820,47	0,49
Threskiornis aethiopicus	Sacred ibis	54,17	9643,49	428,17	0,56
Ardea cinerea	Grey heron	69,61	4999,82	388,49	1,39
Pelecanus erythrorhynchos	American white pelican	105,12	13012,42	356,54	0,81
Fregata magnificens	Magnificent frigate bird	66,31	10402,14	422,33	0,64
Phalacrocorax carbo	Great cormorant	82,2	13440,04	532,23	0,61
Phalacrocorax harrisi	Galapagos cormorant	71,37	10936,73	708,70	0,65
Grus grus	Common crane	166,06	19959,78	1157,67	0,83
Columba livia	Rock dove	14,84	2134,52	222,20	0,70
Creagrus furcatus	Swallow tailed gull	25,22	4927,97	327,71	0,51
Larus argentatus	Herring gull	30,4	5719,9	602,88	0,53
Rhynchops niger	Black skimmer	8,45	1235,81	83,79	0,68
Gelochelidon nilotica	Gull billed tern	17,36	1900,16	182,04	0,91
Stercorarius skua	Skua	53,89	6785,19	402,36	0,79
Alca torda	Razorbill	47,04	3285,72	197,80	1,43
Vultur gryphus	Condor	383,23	27099,93	899,72	1,41

Circus cyaneus	Hen harrier	25,86	3928,72	478,91	0,66
Buteo buteo	Common buzzard	33,22	7856,74	766,82	0,42
Aquila chrysaetos	Golden eagle	104,74	21045,03	1073,30	0,50
Pandion haliaetus	Osprey	80,57	10151,38	556,30	0,79
Sagittarius serpentarius	Secretary bird	124,33	12912,27	1035,56	0,96
Tyto alba	Barn owl	22,65	6522,84	113,50	0,35
Trogon curucui	Blue crowned trogon	6,33	890,72	88,09	0,71
Coracias garrulus	European roller	12,70	1970,03	280,34	0,64
Alcedo atthis	Common kingfisher	8,12	741,51	98,99	1,10
Ramphastos dicolorus	Toucan	34,45	4525,02	466,53	0,76
Falco tinnunculus	Common kestrel	20,17	3154,65	286,44	0,64
Falco subbuteo	Eurasian hobby	18,65	2994,73	256,95	0,62
Amazona aestiva	Blue fronted amazon	35,24	8511,51	305,56	0,41
Ara macao	Scarlet macaw	29,08	15157,87	715,45	0,19
Strigops habroptila	Kakapo	26,06	8849,56	30,09	0,29
Tyrannus tyrannus	Eastern kingbird	1,18	532,71	59,58	0,22
Acanthorhynchus superciliosus	Western spinebill	28,89	2369,64	318,24	1,22
Corvus corax	Raven			1022,46	
Hirundo rustica	Barn swallow	4,08	217,36	33,79	1,88

Podargus strigoides	Tawny frogmouth	14,84	2322,97	239,67	0,64
Selasphorus rufus	Rufus hummingbird	1,64	157,29	17,60	1,04
Apus apus	Common swift	5,25	707,83	50,89	0,74
Steatornis caripensis	Oilbird	14,55	2039,77	103,32	0,71

Brain and FCL endocast segmentation protocol

The data were processed using Amira 5.3.3 (Visualization Sciences Group. France). Processing consisted of five parts: 1) reorientation of the scan to obtain digital skulls in orthogonal anatomical orientation by using the Transform Editor and applying the transformation using a standard interpolation in extended mode and preserving voxel size; 2) bone segmentation by using the Masking tool of the Segmentation Editor to select all bone material in each slice; 3) manual segmentation of the braincase cavity using "Magic Wand" or "Brush" tools; 4) selection of both FCL fossae volumes by using the 3d "lasso" tool – this process consisted of 3 steps: a) making a sagittal cut of the skull which made the periotic area visible; b) selecting the volume inside the fossae; c) cut the volume that exceeds the contour (corresponding to the anterior semicircular canal) that results from the change of angle between the braincase lateral wall and the fossa itself (Walsh et al., 2013) (Figure 2.3); 5) measurement of brain cavity and FCL fossae volumes (combined volume of left and right structures). The FCL fossae volumes were measured trice by different people in order to detect relevant measurement errors. No significant differences were noticed between different measurements. This procedure was applied to all CT scans.

Braincase cavity and FCL fossae volumes for *Monodelphis domestica*. *Didelphis virginiana*. *Phascolarctos cinereus*. *Dasyurus hallucatus* and *Dromiciops gliroides* were obtained from Macrini at el. (2007). I used Castanhinha et al. (2013) values and semicircular canal images of *Niassodon mfumukasi*.

17 skull CT scans were downloaded from the Kyoto University Primate Research Institute's (KUPRI) online collection (http://dmm.pri.kyoto-u.ac.jp/). Although the voxel size of these scans was larger it did not compromise our analysis, because the resolution allowed detection and a detailed segmentation of the FCLs fossae. These specimens were not used to perform measurements with the semicircular canals because scan quality did not allow for an accurate selection of these structures.

Our bird dataset is composed of 59 species of extant birds (Table 2.2). I used published FCL fossae cast and endocast volumes (Walsh et al. 2013). The optic lobes (OL) are part of the

mesencephalon (midbrain) and are especially prominent in birds (Alonso et al., 2004; Kundrát. 2007). which makes them distinguishable and possible to separate from the rest of the brain structures. I used a similar protocol to the one described above for mammals to digitally segment the FCL volumes.

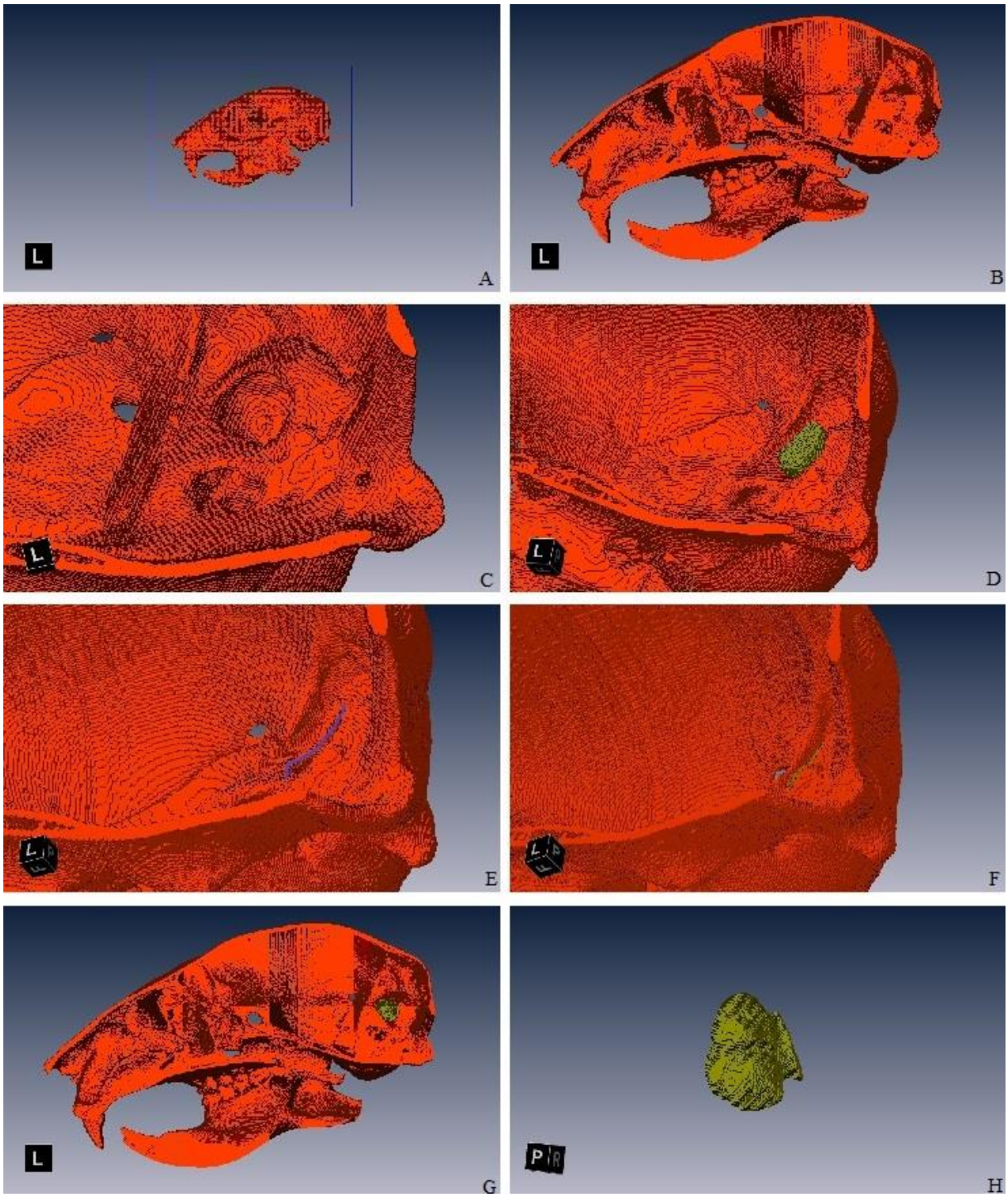

Figure 2.3 – Segmentation process of FCLs: lateral view of a *Sciurus vulgaris* (red squirrel) skull (A); sagittal view after cutting the proximal part of the skull (B); detail of the periotic and the FCL fossa (C); volume of the FCL fossa roughly selected (D); selection of the plane delimiting the fossa (E); extraction of the exceeding volume (F); sagittal view of the skull with FCL fossa volume selected (G); a cast of the FCL fossa (H).

Semicircular canals segmentation protocol

The segmentation of the semicircular canals was only performed on the MfN specimens because the quality of the CT-scans allowed a satisfactory reconstruction of these structures. To improve resolution in some of the smaller animals the original (non-binned) data was used for semicircular canals segmentation. The process was similar to braincase cavity segmentation and consisted of the first three parts of the abovementioned procedure. In most cases, the threshold of the masking tool was adjusted multiple times during semicircular canals manual segmentation. This was important because some parts of these small structures could not be selected with the same threshold values used to segment the braincase cavity. After segmentation, a 3D image of each anterior semicircular canal was created using "SurfaceGen" function with constrained smoothing of the surface and a minimal edge length of 0,4. The surface was displayed with the "SurfaceView" module and the following setting was applied: "Draw style" was defined as *Shaded*, which displays an opaque shaded surface with no visible edges; in "More options", I selected *Opaque*, *Both* faces; the last group options I selected *Direct normals* and used constrained smoothing in the surface rendering.

Then the perspective was changed to orthographic and the "two viewers" option was enabled to allow the visualization of the surface from two different angles. I oriented the anterior semicircular canal on a longitudinal plane on the first camera using the transform editor trackball manipulator to obtain a sagittal view on the second camera because the camera positions are positioned at 90º, (see Figure 2.4). A scale was then created and the background was turned black in order to increase contrast. Then I produced snapshots and opened the resulting images using FIJI (Schindelin et al.. 2012). Using "Set scale" function to define a reference known distance I calibrate them. Then I selected the "Wand" tool and set tolerance to 10 to select the inner area outlined by the anterior semicircular canal (see Figure 2.5). In order to obtain a smoother selection, all the forms were interpolated before being measured using an interval of 20 pixels. I used "Measure" from "Analyze" menu to obtain area and perimeter values.

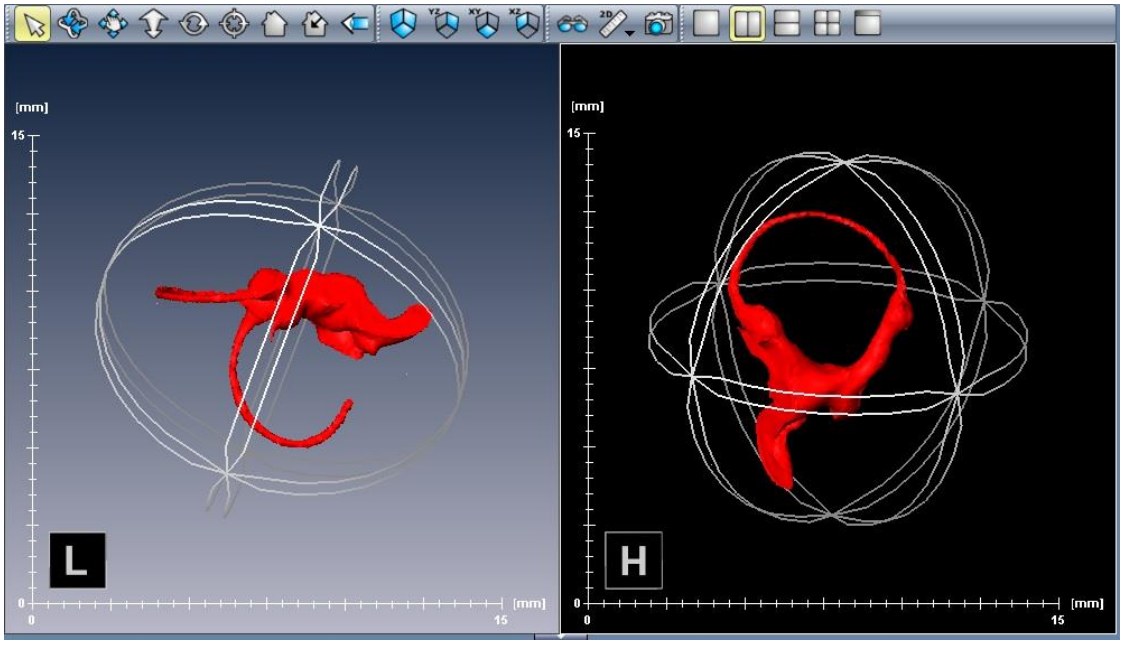

Figure 2.4 – Reorientation process of the anterior semicircular canal of *Ratufa bicolor* (Black giant squirrel) with double view option and "trackball" transformation tool.

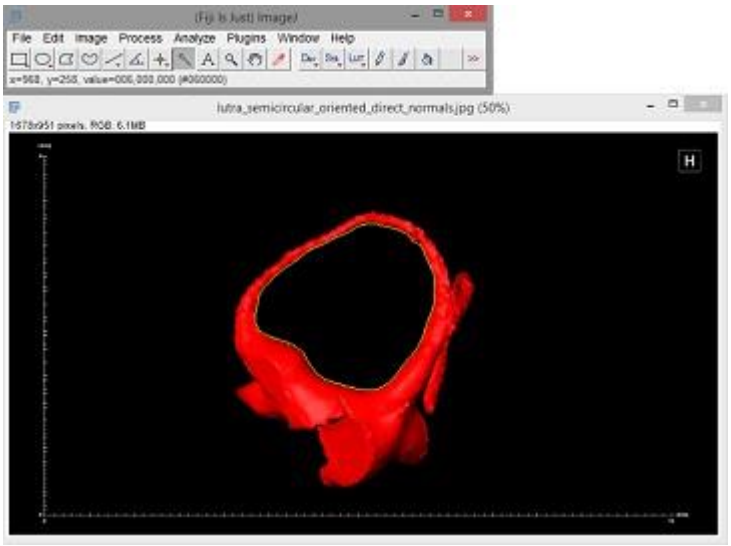

Figure 2.5 – Measurement of a *Lutra lutra* (European otter) anterior semicircular canal area and perimeter.

Statistical analysis

To obtain relative values for FCL, optic lobes and anterior semicircular canal areas I performed a log 10 transformation on the original FCL, optic lobes (OL), Total Endocast Volume minus FCL (BrainR) and Total Endocast Volume minus optic lobes (Brainr), anterior semicircular canal areas (ASC) and calculated phylogenetic residuals from linear phylogenetic regressions on: FCL and BrainR for mammals and birds; OL and Brainr for birds; ASC and BrainR. To calculate these residuals I used R package phytools (v 0.3-72) that fits phylogenetic regressions and computes the residuals which was designed for phylogenetic size correction using GLS regression (Revell, 2009). This package requires the input of a dependent (e.g., FCL volume) and at least an independent variable (e.g., BrainR volume) as well as a phylogenetic tree (see below) in R's "phylo" format which can be loaded both on Nexus or Newick file formats. The phylogenetic residuals obtained were used as relative FCL, OL and ASC size in the subsequent analyses. Residuals were analyzed and normality was tested, following Butler et al. (2000), using histograms, Q-Q plots and Shapiro-Wilk normality tests. In all situations I used PDAP package (Garland et al.. 1993) in Mesquite 3.03 (Maddison & Maddison. 2009) to run phylogenetically correct regressions and map the prediction intervals onto the original tip data space (see Figures 2.6, 2.7, 2.8) to detect the existence of outliers before the analyses (Garland & Ives. 2000). For OL relative values calculation *Apteryx haasti* (great spotted kiwi) and *Strigops habroptila* (kakapo) were dropped because they were significant outliers, i.e., they fell out of the phylogenetic prediction interval. Body mass values for birds were obtained from Walsh et al. (2013) and from Felisa et al. (2003) for mammals. These values were also log 10 transformed.

I built a phylogenetic tree (Figure 2.9) based on the topology of Meredith et al. (2011). Mesquite 3.03 was used to build the tree and modify branch lengths. I used divergence time as branch lengths and data was collected from several publications. Spoor et al. (2007) was used for higher taxonomic levels. while divergence times that separate families and genera were collected from the following works: Meredith et al. (2008) for Marsupialia; Arnasson et al. (2008) and Poux et al. (2008) for Afrotheria; Nyakatura & Bininda-Emonds (2012) for Carnivora; Agnarsson et al. (2011) for Chiroptera; Steppan et al. (2004) and Blang-Kanfi et al. (2009) for Rodentia; Perelman et al. (2011) for Primates. *Niassodon mfumukasi* was added as outgroup to all the other clades and the divergence time between Anomodontia and Theriodontia (the clade in which class Mammalia is included) was fixed at 261 million years. The most primitive anomodonts were found in Dashankou locality (Liu et al., 2009) in China. There are no theriodonts in Dashankou and, therefore, I assume that divergence happened before the Lower *Pristerognathus* zone. Given that no dating is available, we consider Rubidge et al. (2005) U-Pb dating of 261 million years as a minimum age for divergence. The phylogenetic tree for birds data set was pruned using R drop.tip() function of package ape which allowed the selection of 59 of the 9872 species in the original tree file from Hedges et al. (2015) (Figure 2.10). The original tree had divergence time (million years) as branch lengths.

I divided the data set in ecological categories related to feeding, activity pattern, dimension of locomotion and locomotor type.

For both birds and mammals I classified them according to:

1. Feeding strategy - (0) gatherer. (1) occasional predator. (2) predator - in which gatherers do not engage in any kind of predation. occasional predators predate but are predominantly omnivores and predators which obtain most of their resources by hunting;
2. Activity pattern – (0) nocturnal. (1) nocturnal/diurnal. (2) diurnal - being nocturnal/diurnal category for those animals which do not fit a strictly nocturnal or diurnal pattern.

Additionally, I created 3 more divisions for our mammalian data set:

1. Dimension of locomotion – (0) 2D, (1) 3D - in which groups include animals which move mainly on a horizontal plane and which consistently move both horizontally and vertically;
2. Locomotor type – (0) fossorial, (1) semiaquatic, (2) terrestrial, (3) scansorial, (4) arboreal, (5) flyer – adapted and modified from Van Valkenburgh (1985), fossorials forage and shelter underground, semiaquatics forage on water but shelter on dry land or built platforms, terrestrials forage and shelter on the ground and rarely or never climb, scansorials move on the ground but regularly climb, arboreals forage and shelter on trees;
3. Agility – (0) slow, (1) medium slow, (2) medium, (3) medium fast, fast (4) – adapted from Spoor et al., 2007.

Analyses of variance were performed to find out if there are significant differences in FCL relative size of the created categories. The data was assembled on a *.csv file and loaded to R software to check for collinearity issues between predictors (Mundry, 2014). R packages car. MASS and nnet were used. In the case of mammals, a large Generalized Variance Inflation Factor was revealed for locomotion dimension and locomotor type. Therefore as an internal control I ran multiple regressions with and without these predictors in the model to see if they were influential in our results. The results were not altered.

I performed Phylogenetic Generalized Least-Squares (PGLS) analyses, a type of regression that takes into account the phylogenetic relationships between tip data (Grafen, 1989; Lavin et al.; 2008; Gartner et al., 2010). I exported tip data and covariance matrices from the built phylogenetic tree in ASCII text file format using PDTREE.EXE and PDDIST.EXE from Mesquite and used Regressionv2.m to perform all the calculations on MATLAB (Lavin et al., 2008). Multiple regressions were performed using a PGLS with ultrametric trees with divergence time (million years) as branch lengths. In the case of the mammalian analyses the tree was not ultrametric due to the presence of a fossil specimen. I also performed a PGLS with all branch lengths set to 1 as in Walsh et al. (2013).

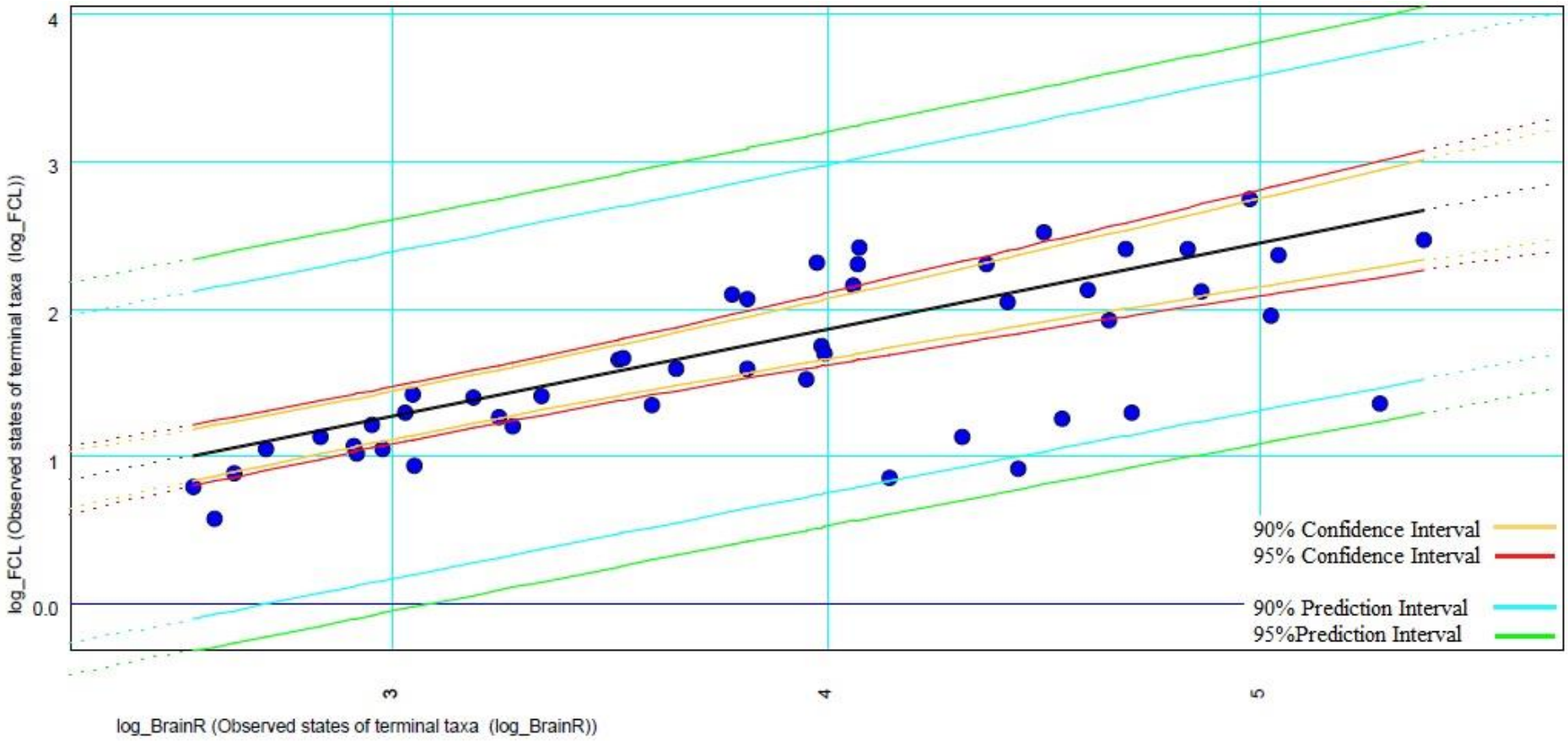

Figure 2.6– Mammals plot of phylogenetically correct regression of Log10 transformed BrainR (*x* axis) and Log10 transformed FCL (*y* axis) values from specimens in table 2.1. All specimens lie within the 95% prediction interval. *Felis catus* and *Puma concolor* are the two specimens falling closer to the 95% prediction interval lower limit.

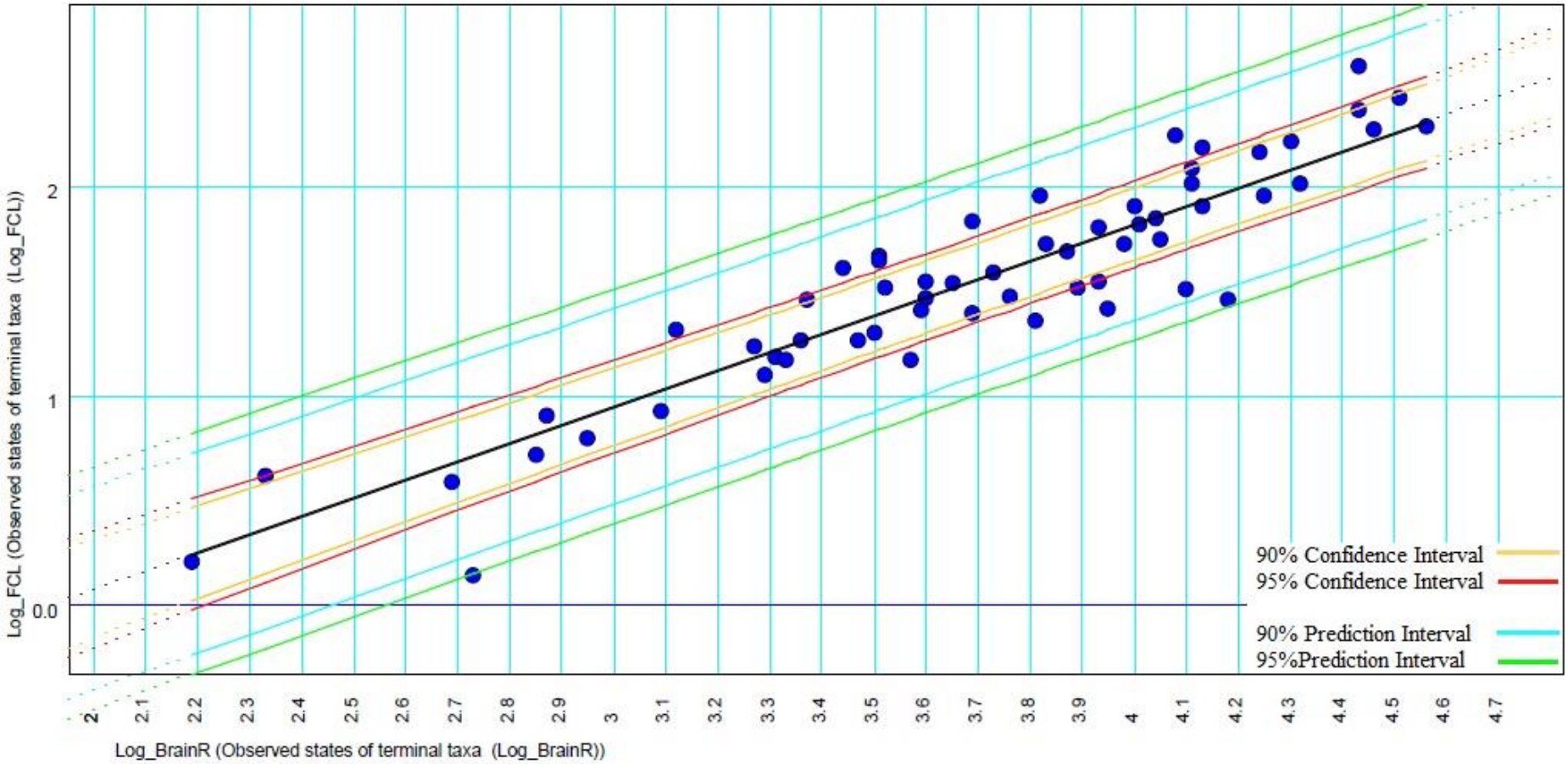

Figure 2.7– Birds plot of phylogenetically correct regression of Log10 transformed BrainR (*x* axis) and Log10 transformed FCL (*y* axis) values from Walsh et al. (2013). All specimens lie within the 95% prediction intervals except fot *Tyrannus tyranus* which is slightly outside the 95% prediction interval.

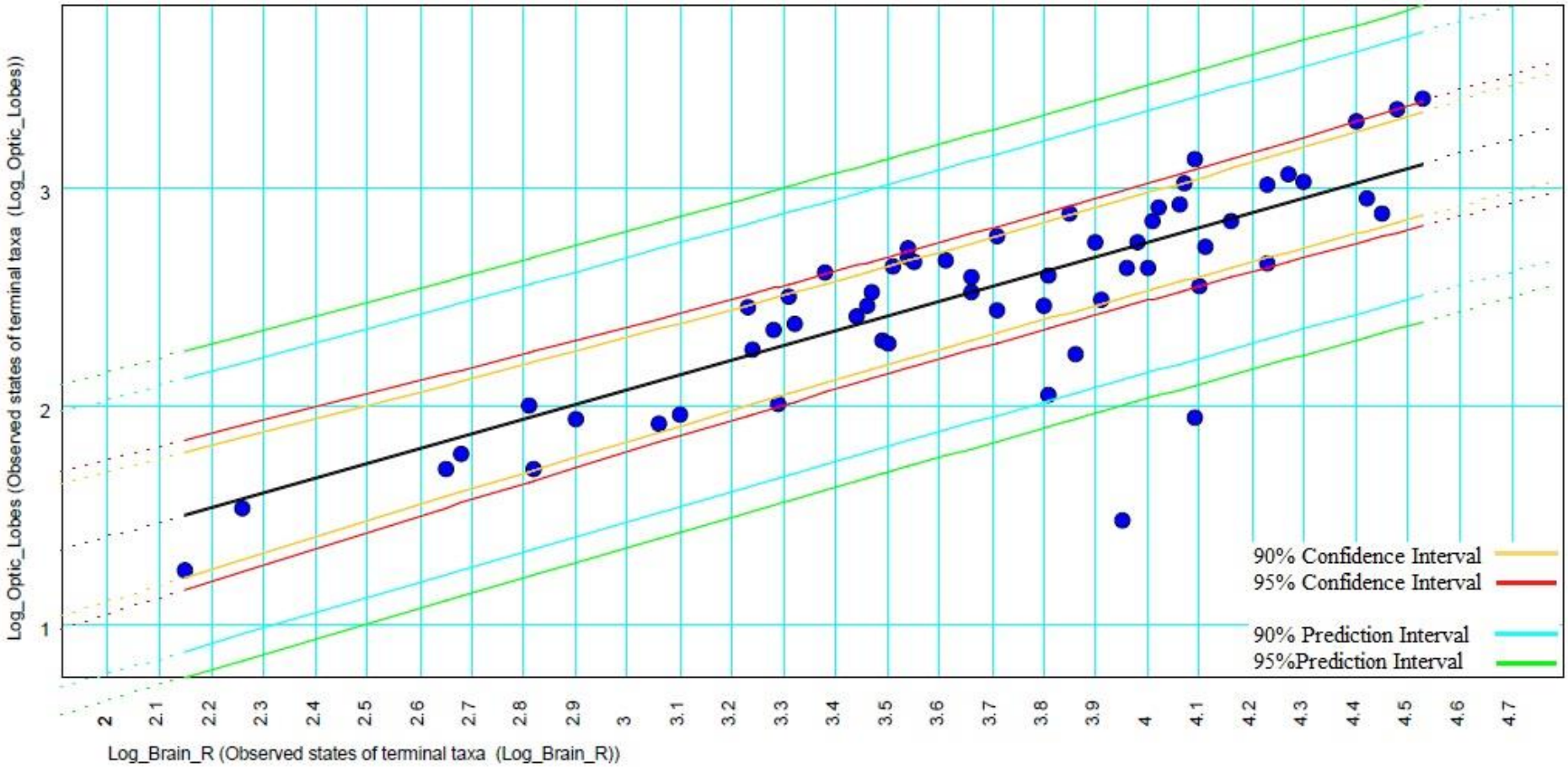

Figure 2.8 - Birds plot of phylogenetically correct regression of Log10 transformed BrainR (*x* axis) and Log10 transformed OL (*y* axis) values. OL and Brainr were measured with the same data from Walsh et al. (2013). *Strigops habroptila* and *Apteryx haasti* fall outside the 95%prediction interval.

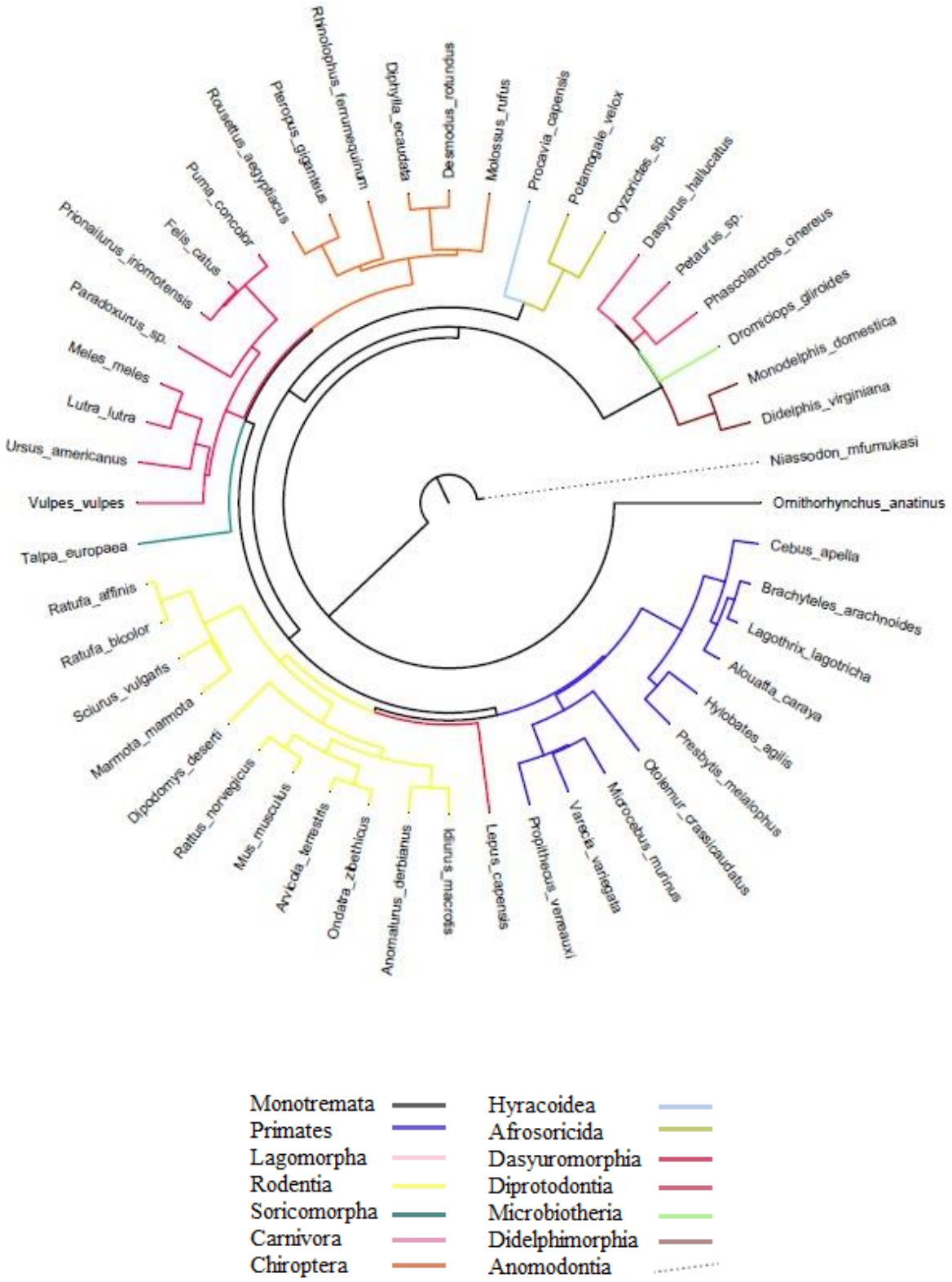

Figure 2.9 – Mammalia phylogenetic tree used in this study based on Meredith et al. (2011). Colours represent different orders.

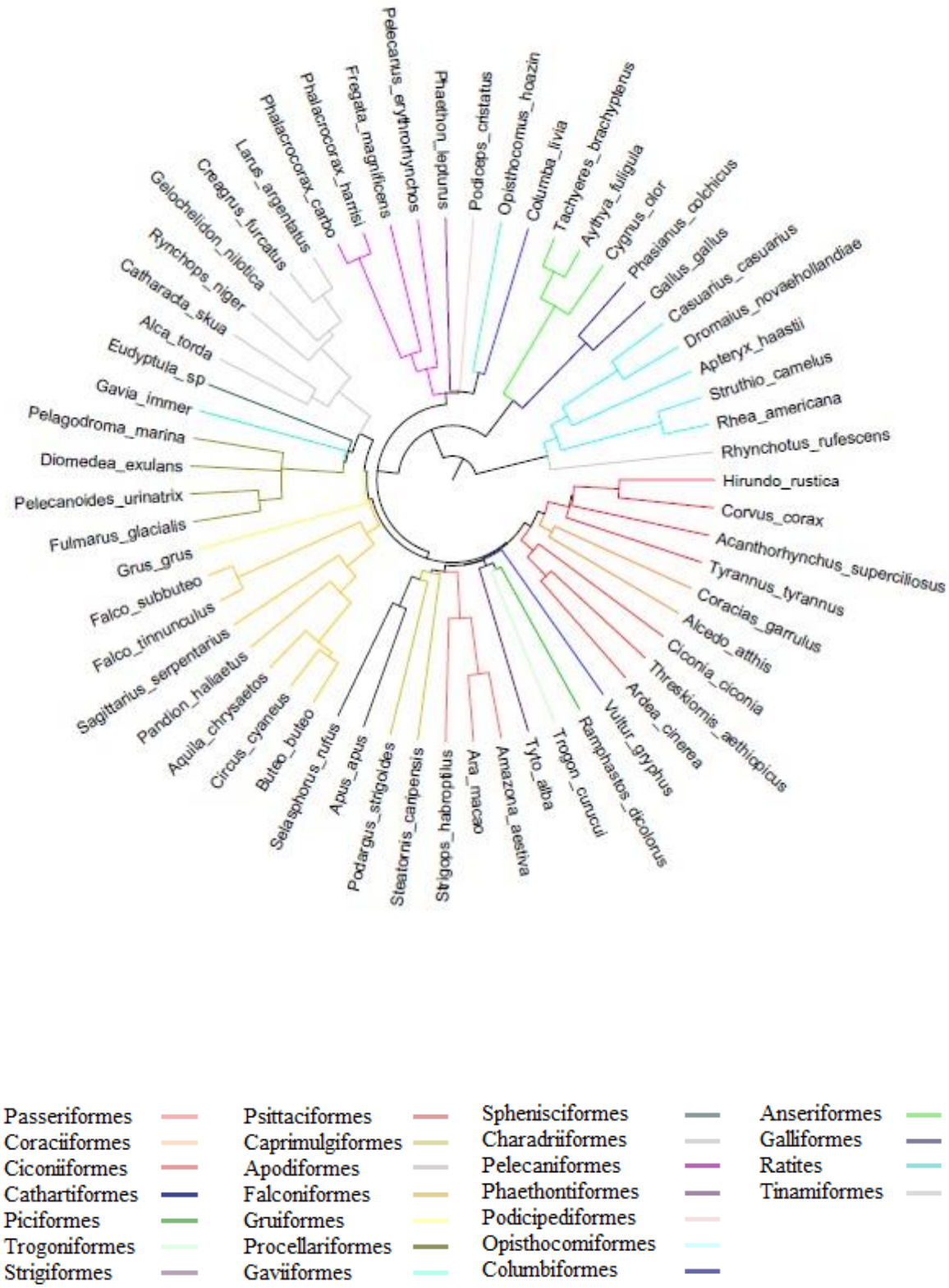

Figure 2.10 – Bird phylogenetic tree used in this study based on Hedges et al. (2015). Colours represent different orders.

Results

Mammals

In absolute terms, the specimen with the largest FCL fossae volume of our data set is the *Lagotrix lagotricha* (Humboldt's wolly monkey) with 460.74 mm^3 and the specimen with the smallest FCL fossae volume is the *Mus musculus* (house mouse) with 3.70 mm^3. Proportionally, the specimen with the largest FCL fossae volume value is the *Talpa europaea* (European mole) with 2.42% of the total brain endocast and the smallest value belongs to *Vulpes vulpes* (red fox) at 0.03%. However, the relative FCL fossae volume values obtained from an ordinary least-squares regression show *Lepus capensis* (Cape hare) as the largest relative FCL size while *Puma concolor* (cougar) is the smallest.

There is no significant correlation between FCL relative size and bodymass (all p values >0.13). Agility categories do not separate species according to FCL relative sizes (all p values >0.19). The FCL relative size does not vary with locomotion dimension (all p values >0.24) and locomotor type (all p values >0.12). The results remained unaltered when "fossorial" category (which had only 2 specimens) was removed from the analysis. The analysis revealed no difference between activity pattern (p value >0.13) and feeding categories (p value >0.37). When "Diurnal/Nocturnal" category was removed from the analysis the results did not change. The analysis of scatterplots reveals considerable variability within each ecological category (Figures 3.2, 3.3, 3.4, 3.5, 3.6). See table 3.1 for analyses result details.

In what concerns the relative area of ASCs, I found no significant correlation with FCL relative size (p value>0.18, table 3.2, Figure 3.7). I also tested a correlation with ASCs perimeter, but it was also non-significant (table 3.2).

Table 3.1 – Results of the analyses of variance of the mammal data set. Statistics of the effect of each predictor on FCL relative size variation (F-test value, degrees of freedom and p value).

	Divergence time tree	**Equal branch length tree**
Body mass	F = 0.78, df = 1, 32, p = 0.38	F = 2.47, df = 1, 32, p = 0.13
Locomotion dimension	F = 1.44, df = 1, 32, p = 0.24	F = 0.32, df = 1, 32, p = 0.58
Activity pattern	F = 1.34, df = 2, 32, p = 0.28	F = 2.14, df = 2, 32, p = 0.13
Feeding	F = 0.93, df = 2, 32, p = 0.41	F = 1.03, df = 2, 32, p = 0.37
Locomotor type	F = 0.73, df = 5, 32, p = 0.61	F = 1.93, df = 5, 32, p = 0.12
Agility	F = 0.57, df = 4, 32, p = 0.69	F = 1.65, df = 4, 32, p = 0.19

Table 3.2 - Results of the analyses of variance of the mammal data set. Statistics of the effect of ASC relative area and perimeter on FCL relative size variation (F-test value, degrees of freedom and p value).

	Divergence time tree	**Equal branch length tree**
ASC relative area	F = 1.80, df = 1, 24, p = 0.19	F = 1.89, df = 1, 24, p = 0.18
ASC relative perimeter	F = 1.32, df = 1, 24, p = 0.26	F = 1.42, df = 1, 24, p = 0.24

Birds

The specimen with the largest optic lobes absolute volume is the *Struthio camelus* (ostrich) with 2585.47 mm^3, while *Selasphorus rufus* (rufus hummingbird) had the smallest volume (17.60 mm^3). Proportionally, *Hirundo rustica* (barn swallow) had the largest optic lobes relative size (15.54%) and the smallest value is observed in *Strigops habroptila* (0.34%). *Phaethon lepturus* (white-tailed tropicbird) has the largest relative optic lobes value and *Tyto alba* (barn owl) has the smallest, according to the residuals from an ordinary least-squares regression (see Materials and Methods).

Our analysis on bird data revealed no significant correlation between FCL relative size and body mass (all p values >0.31). The analysis of variance showed a difference in average relative size of nocturnal and diurnal birds (all p values <0.03) and feeding categories (all p values >0.02) (Figures 3.8, 3.9). When OL relative size was added to the analysis, no significant correlation with between FCL was obtained when using the divergence times tree (p = 0.16) but the equal branch tree returned a marginally significant result (p = 0.04) (see table 3.3).

Table 3.3 - Results of the analyses of variance of the bird data set. Statistics of the effect of each predictor on FCL relative size variation (F-test value, degrees of freedom and p value).

	Divergence time tree	**Equal branch length tree**
Body mass	F = 2.22, df = 1, 54, p = 0.14	F = 2.81, df = 1, 54, p = 0.09
Feeding	F = 4.69, df = 2, 54, p = 0.01	F = 4.07, df = 2, 54, p = 0.02
Activity pattern	F = 7.81, df = 1, 54, p < 0.01	F = 8.98, df = 1, 54, p < 0.01
Optic Lobes	F = 2.02, df = 1, 51, p = 0.16	F = 4.32, df = 1, 51, p = 0.04

In sum, FCL relative size differs from feeding and activity pattern categories in birds. In mammals, no significant result was yielded for ecological categories. Both in mammals and birds, FCL relative size does not correlate with body mass.

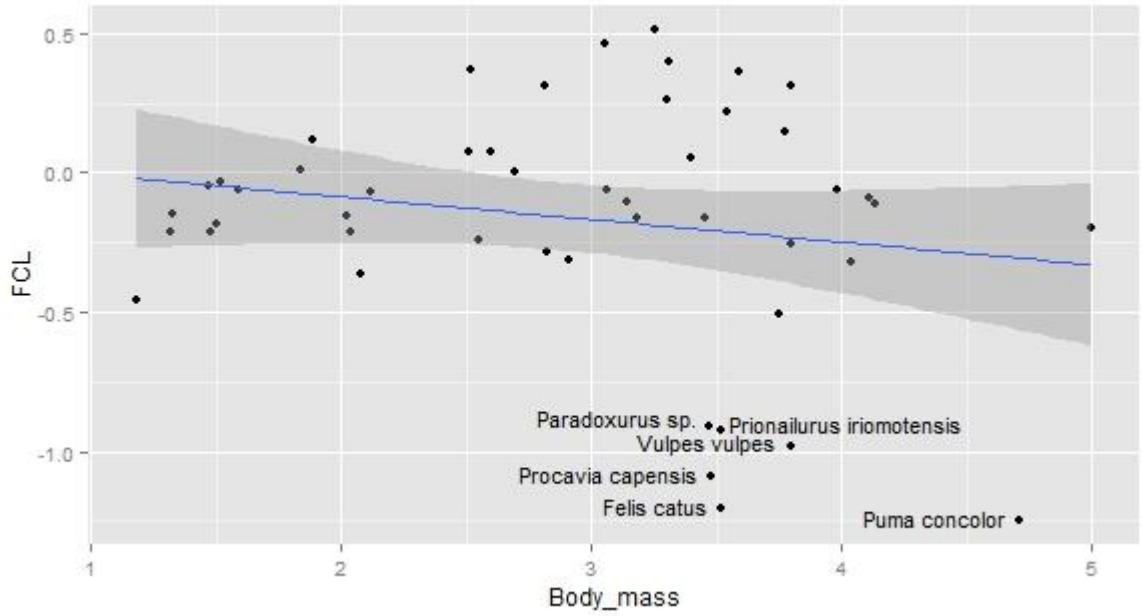

Figure 3.1 – Mammals data scatterplot set with *x* = log10 body mass and *y* = FCL relative size. The blue line is an ordinary least-squares regression line and the grey area is the 95% confidence interval. Note six severe outliers in the bottom.

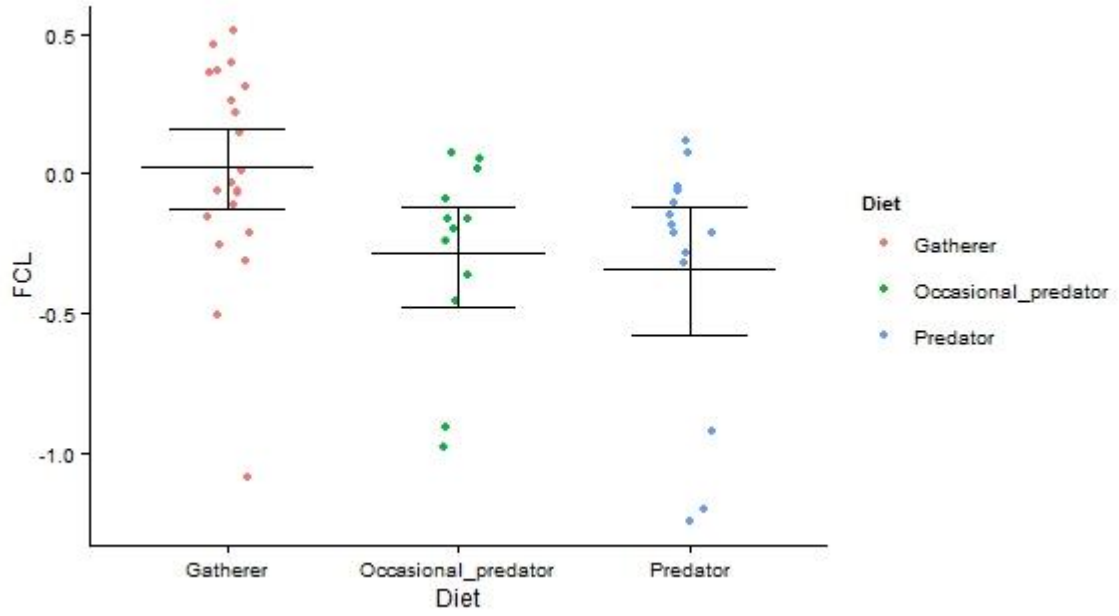

Figure 3.2 – Mammals data scatterplot set with *x* = feeding ecology and *y* = FCL relative size (residuals). For each category, error bars are presented. Both categories have some severe outliers like *Procavia capensis* (Gatherer), *Paradoxurus* sp. and *Vulpes vulpes* (Occasional predator), *Puma concolor*, *Felis catus* and *Prionailurus iriomotensis* (Predator)

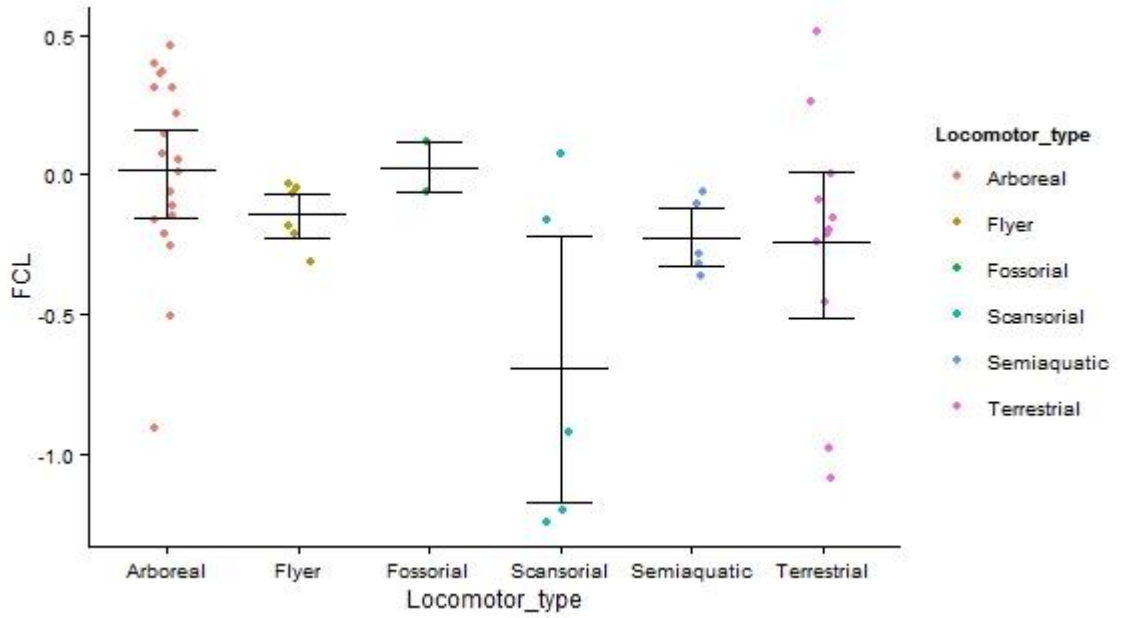

Figure 3.3 – Scatterplot of the mammals data set with *x* = locomotor type and *y* = FCL relative size (residuals). For each category, error bars are presented. Note the variability of Arboreal, Terrestrial and Scansorial categories.

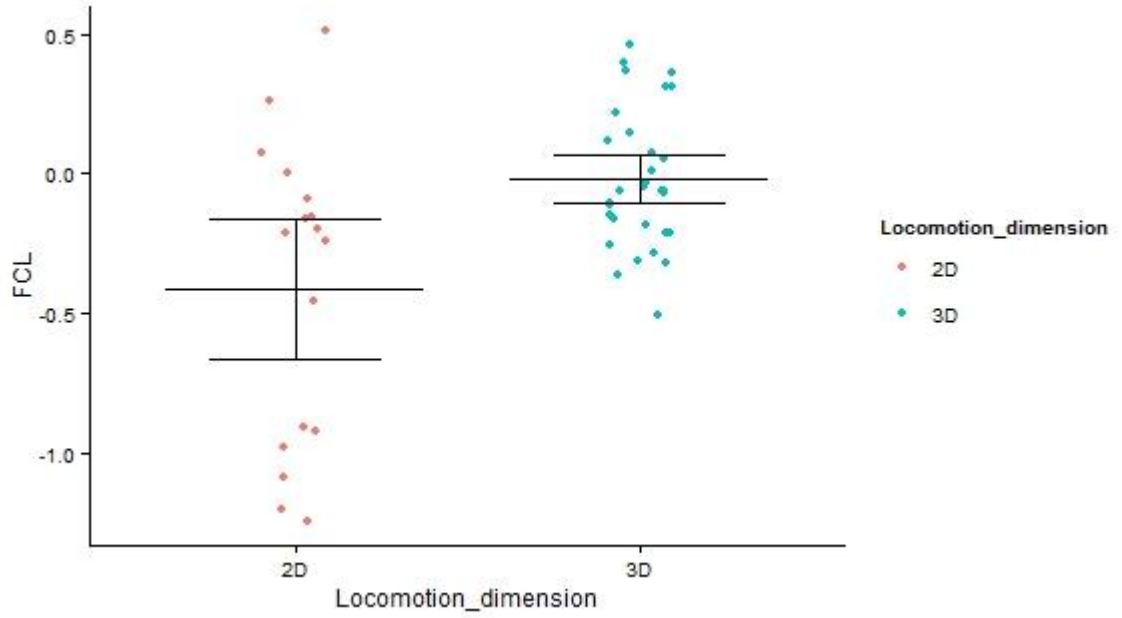

Figure 3.4 – Scatterplot of the mammals data set with *x* = locomotion dimension and *y* = FCL relative size (residuals). Note the variability within the 2D category.

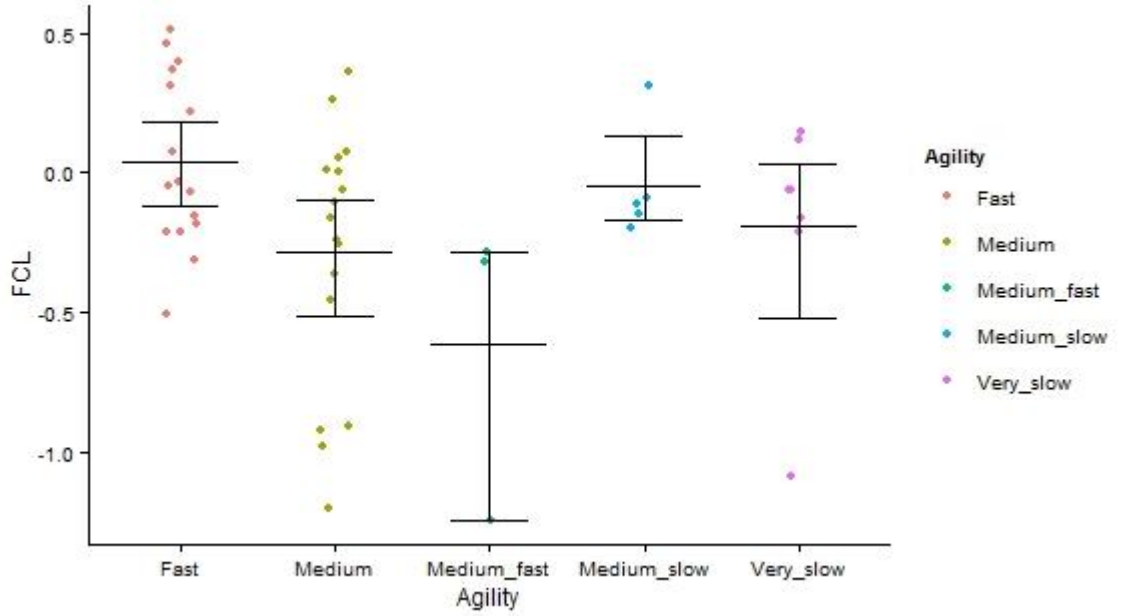

Figure 3.5 – Scatterplot of the mammals data set with *x* = agility and *y* = FCL relative size (residuals). For each category, error bars are presented. Note the outlier in the Very Slow category, *Procavia capensis*. Medium category present highly variable values.

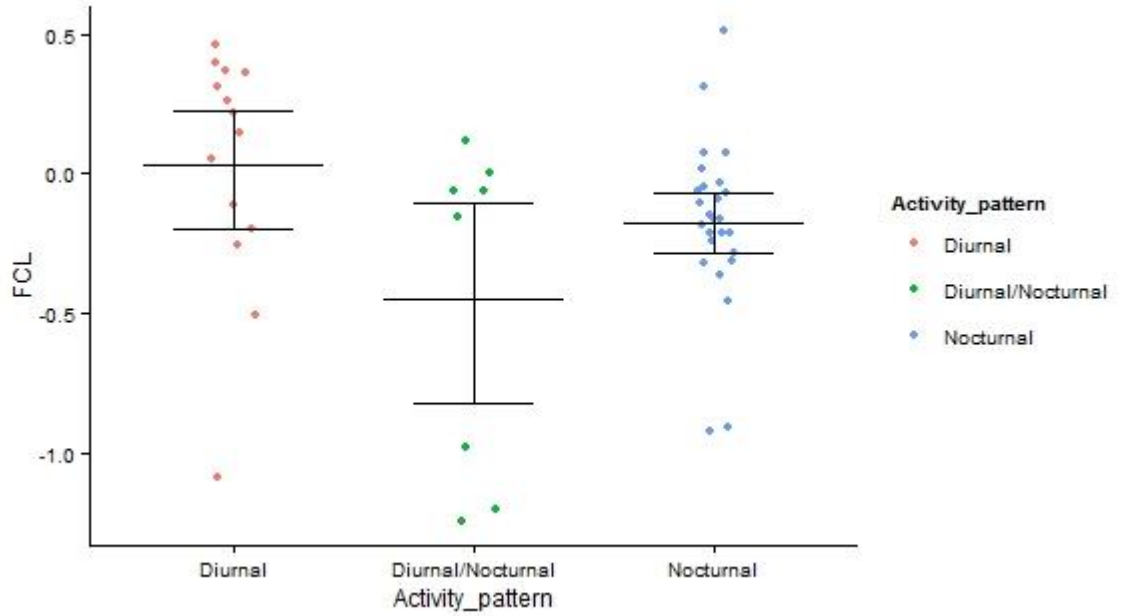

Figure 3.6 – Mammals data Scatterplot of the set with *x* = circadian activity pattern and *y* = FCL relative size (residuals). Values in all categories are highly variable.

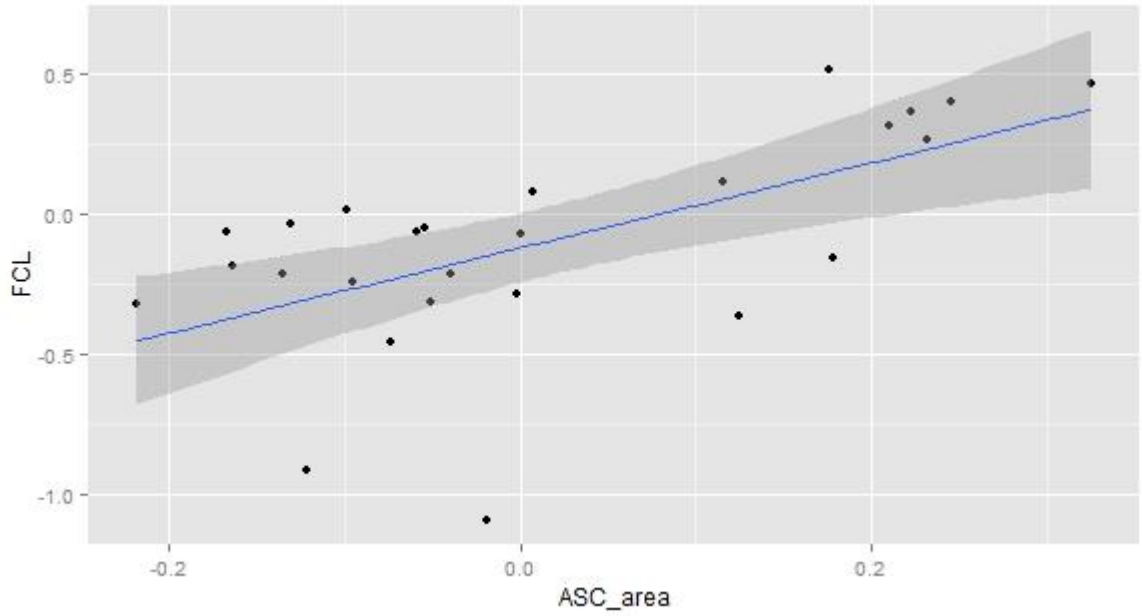

Figure 3.7 – Mammals data scatterplot set with *x* = anterior semicircular canal relative area and *y* = FCL relative size. The blue line is an ordinary least-squares regression line and the grey area is the 95% confidence interval. The most severe outlier, in the bottom, is *Procavia capensis*.

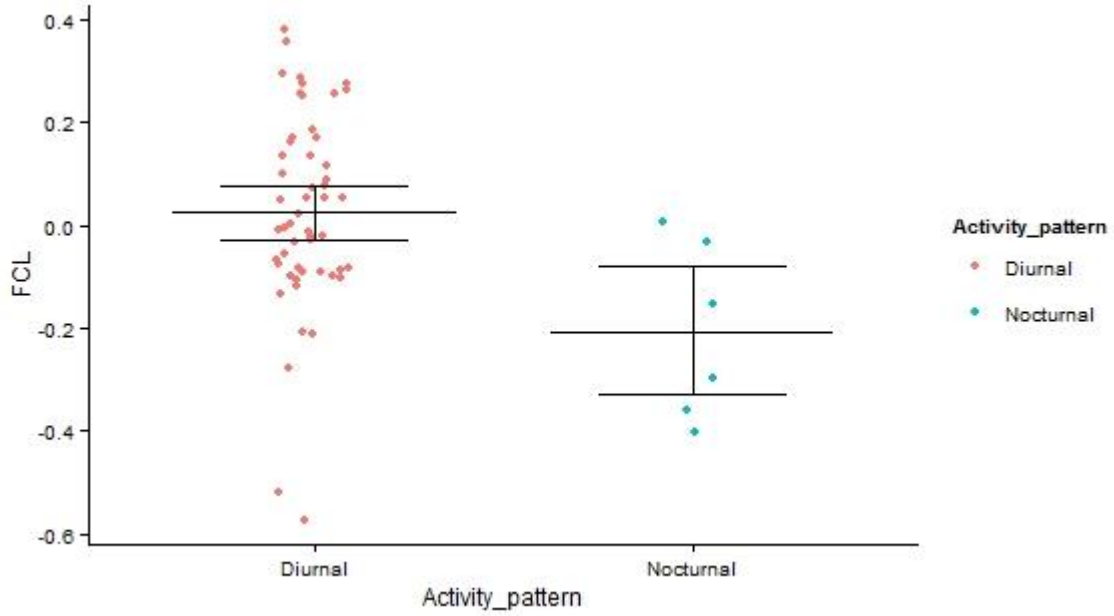

Figure 3.8 – Birds data scatterplot of the set with *x* = circadian activity pattern and *y* = FCL relative size. The Diurnal category has variable values. *Tyrannus tyrannus* and *Ara macao* are severe outliers in the Diurnal group.

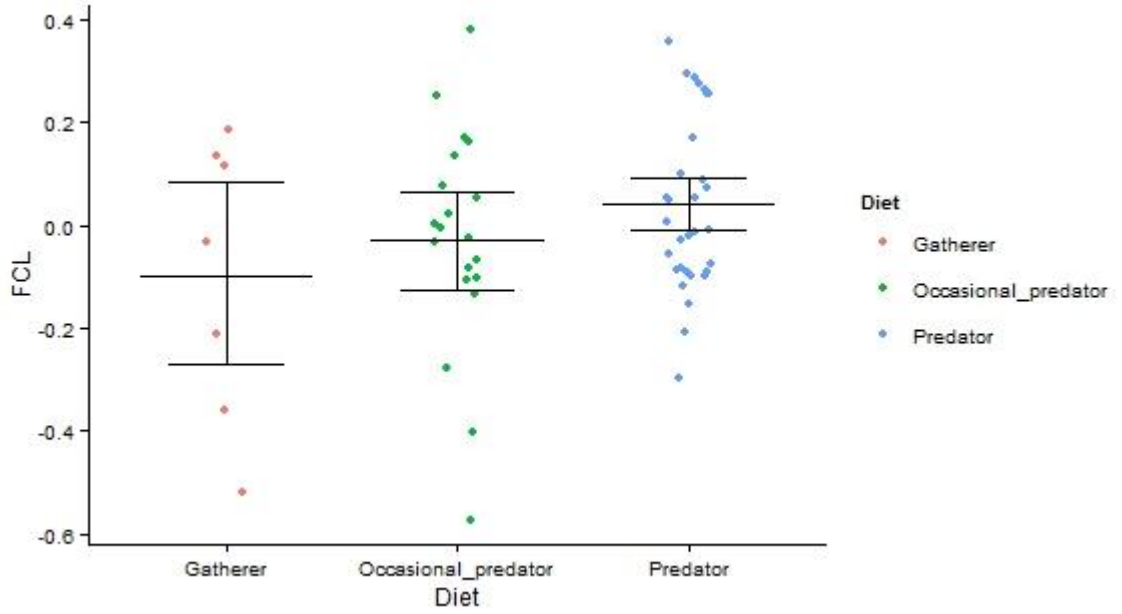

Figure 3.9 – Birds data scatterplot set with *x* = feeding ecology and *y* = FCL relative size. For each category, error bars are presented. Values are highly variable within categories.

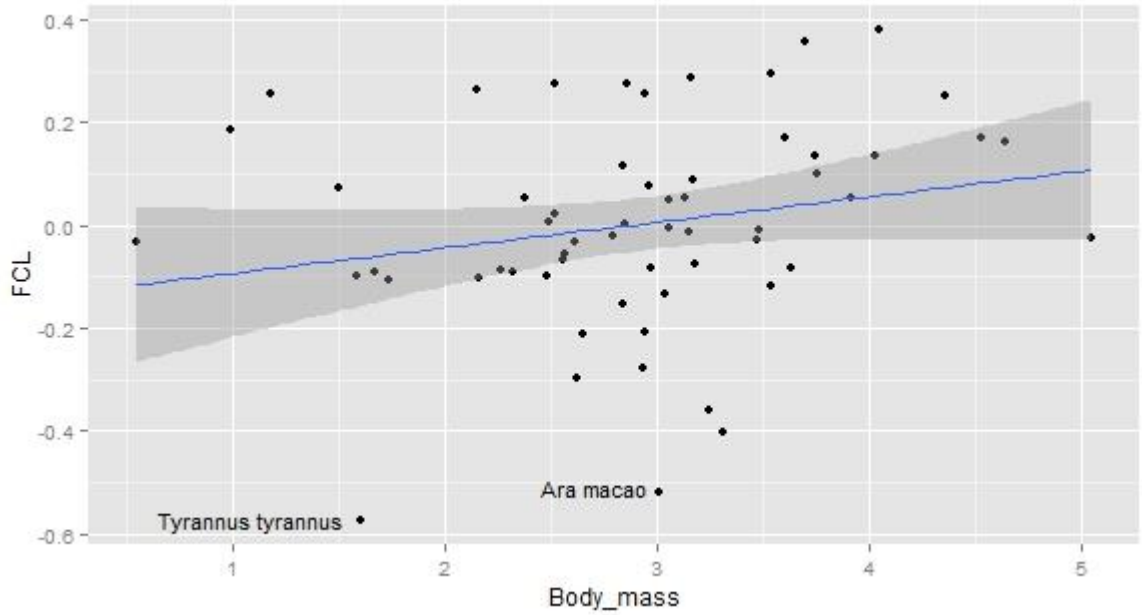

Figure 3.10 – Birds data scatterplot set with *x* = body mass and *y* = FCL relative size. The blue line is an ordinary least-squares regression line and the grey area is the 95% confidence interval. *Tyrannus tyrannus* and *Ara macao* are severe outliers.

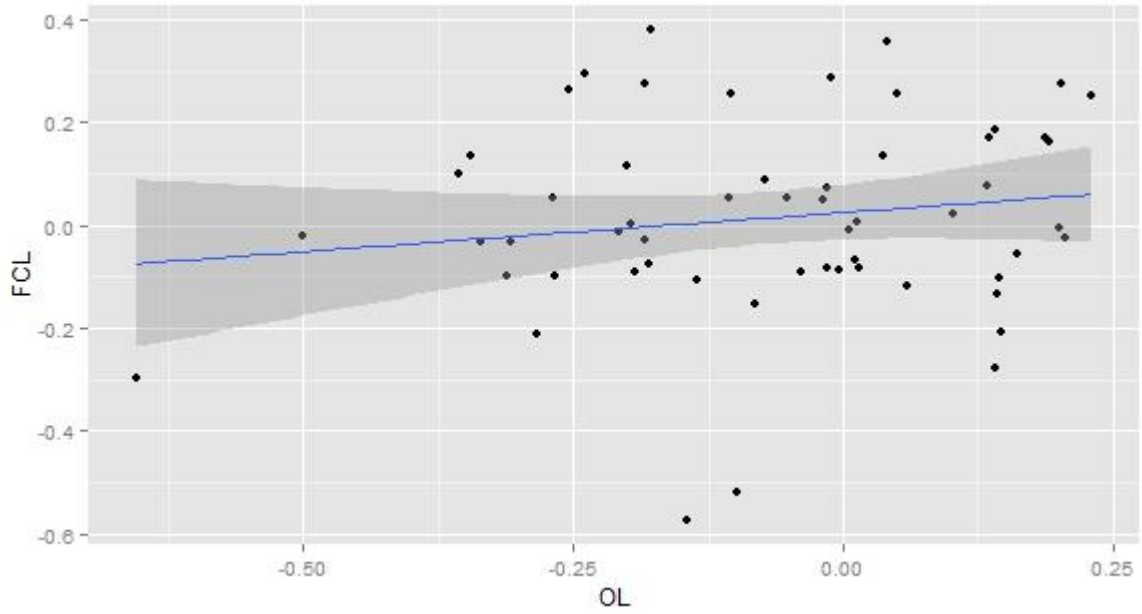

Figure 3.11 – Birds data scatterplot set with *x* = OL relative size and *y* = FCL relative size. The blue line is an ordinary least-squares regression line and the grey area is the 95% confidence interval.

Discussion

General considerations

Despite the apparent simplicity of cerebellar functions, cerebellar structures interaction is complex. This fact implies that strong evidence must be provided before we can establish simple structural-functional correlations. Optimal ocular motor coordination involves several cerebellar areas (Kheradmand & Zee, 2011), thus, it is an oversimplification to isolate individual components (such as the FCL) and link them to specific functions. The FCL controls fast-acting and immediate movements as holding images steady and smooth pursuit or VOR while the nodulus/uvula complex is responsible for orientation of images in the retina. On the other hand, Walker et al. (2008, 2010) shows that lesions in the nodulus/uvula complex also affect the efficiency of high-frequency translational-VOR and smooth pursuit. Moreover, other parts of the cerebellum (dorsal vermis and the posterior fastigial nucleus) also play a role in smooth pursuit (Fuchs et al., 1994; Takagi et al., 2000; Kheradmand & Zee, 2011). Hence, besides the FCL there are other parts of the cerebellum that control the VOR, smooth pursuit or VCR. This functional redundancy may have had obvious adaptive functions, which can help in the interpretation of the results. Although results do not find a correlation between the FCL relative size and ecology that does not mean ecological traits are not related with ocular motor accuracy. Instead, I may be distorting the analysis by underestimating the cerebellar tissue involved in a certain function, by assigning oculomotor functions solely to the cerebellar tissue inside the FCL fossae. Because accurate discrimination and segmentation of cerebellar structures (other than those resting in fossae and foramina) in endocasts is difficult (Lyras, 2009), results may be biased and conclusions distorted.

Despite Nagao (1992) and Nagao et al. (1997) show functional differentiation between the flocculus and paraflocculus, Rambold et al. (2002) findings do not support a functional compartmentalization. This raises doubts about the assumption that large FCLs is a *sine qua non* condition for efficient eye motor control throughout brain evolution. Taking this into account, it would be important to study structures that are directly connected to FCLs, like the semicircular canals. McVean (1999) refers that the canal lumen area of *Talpa europaea* (European mole) is relatively larger than that of *Rattus norvegicus* (brown rat). Considering the fact that eyes of cave dwelling animals may degenerate (Behrens et al., 1997), the sluggish and visionless life habit of moles could lead to a selective pressure for semicircular canals size reduction. (McVean, 1999). Although, the increase in canal dimensions could mean an increasing importance of vestibular cues, since the animal is devoid of visual cues. If this is true, an increase in FCL size could mean that the function of this part of the cerebellum could be coopted to a different function and, despite the loss of vision, maintain or even increase its size. Considering the origin of the cerebellum and the plasticity of the structure, this hypothesis could be worth of testing by, for instance, the ablation of FCLs in moles. The study of the

effects caused by lesions in non-visual animals would give cues on a possible functional variability in vertebrate FCLs.

By looking in detail to the data, some FCL relative values are difficult to interpret. For instance, *Talpa europaea* (European mole) has relatively large FCL relative values, similar to those of gliding or arboreal species (e.g., *Petaurus* sp. the flying phalanger or *Cebus apella* the tufted capuchin). Yet, moles are practically blind and not particularly agile. The fact that the FCL relative values are high could be related to locomotion in three dimensions while building tunnels both horizontally and vertically. However, as we saw above, the analysis on locomotion dimension retrieved no significant results.

It is also hard to explain why there is not a clear division between FCL relative values of echolocating vs non-echolocating bats. The non-echolocating *Pteropus giganteus* is the bat with the lowest FCL relative values while the also non-echolocating *Roussettus aegyptiacus* has the highest. Echolocating bat values lie in between. It is counterintuitive that sound-oriented animals have structures dedicated to image processing. Witmer et al. (2003) suggested that membranous wings could have sent proprioceptive fibers to the central nervous system in pterosaurs and this might explain the large FCL in pterosaurs. If this is true, we would expect to see a similar pattern on the brains of Chiroptera. However, even if in echolocating bats the FCL does not control image stabilization in the retina, it is more likely that it has a role in integrating vestibular input. It would be important to test possible relationships between FCL size and the diameter of the eye socket, the diameter of optic nerves or the muscle mass in the neck region. All this correlations could provide additional evidence about which function the floccular tissue is doing in each animal.

Although the optic lobes are relatively conspicuous in birds, it is not possible to determine with an endocast to which extent their cerebral tissue is present in a more interior position of the brain. This methodological caveat might have resulted in over- or underestimation of the values of these structures in some species. Nevertheless, endocasts have an inherent limitation because I delimitated cranial structures, not the actual brain. It is therefore impossible to know how much floccular complex is outside the fossa in each species.

In what concerns birds feeding strategies, it is important to refer that some herbivore theropods present apparently relatively large FCL fossae (Kúndrat, 2007). Although it is out of the aim of this work, I propose a future analysis of this group. A global analysis of extinct non-avian theropods is worth, because they occupied different ecologic niches.

Table 4.1 – Summary of the hypotheses testing for mammals and birds data sets. *tested in Walsh et al. (2013); **data not available.

	Mammals	Birds
H I (Body mass vs. FCL size)	Not correlated	Not correlated
H II (Agility vs. FCL size)	Not correlated	Not tested*
H III (Locomotion vs. FCL size)	Not correlated	Not tested*
H IV (Feeding vs. FCL size)	Not correlated	Verified
H V (Optic lobes size vs. FCL size)	Not tested**	Not correlated
H VI (Circadian activity pattern vs. FCL size)	Not correlated	Verified
H VII (Anterior SCC dimensions vs. FCL size)	Not correlated	Not tested**

Mammals

The results here presented suggest that the FCL relative size is not a reliable predictor of ecology and behavior in mammals.

Hypothesis I: Body mass *vs.* FCL size

In the mammals data set, I found no significant correlation between FCL relative size and body mass. I expected, as previously verified in primates (Gannon, 1988), that larger animals would have relatively smaller FCL fossae. Given the functions of the FCLs it was expected that smaller, lighter and more agile mammals would have a relatively larger amount of floccular tissue and therefore a relatively larger fossa. FCL relative size does not present a significant downward trend when body mass increases in the data set. Therefore, although an apparent significant negative correlation between body mass and FCL size in primates, that appears not to be the case when a broader mammalian set is analyzed. It would be important to analyze mammals at the order taxonomic level to understand if, within closely allied groups, a trend exists.

Hypothesis II: Agility *vs.* FCL size

I found no significant difference between FCL relative size values in distinct agility categories. Presence or absence of FCLs is frequently related with a respectively more or less active life style, independently of the taxa. FCL fossae were observed in theropod dinosaurs (Franzosa, 2004), hadrosaurs (Thomas, 2015), ankylosaurs (Carabajal, 2014), pterosaurs (Witmer et al., 2003), and suggestions about their size and agility were not tested. Fossil data is not reliable to test such hypotheses because preserved skull material is scarce and techniques to obtain volumetric data are expensive. After Walsh et al. (2013) presented evidence on the absence of a relation between agility in birds and FCL relative size, it was important to test this putative relation in mammals, a group where

FCL fossae also appear. Our hypothesis was rejected and that is not surprising because recent studies (see Introduction) point for similar functions of the FCL in birds and mammals. As Walsh et al. (2013) discusses, there is a chance that the protrusion of the FCL is a result of an increase in nodulus/ventral uvula size, of bipedalism (due to a more unstable body position), of a large degree of plasticity (for VOR adaptation to distinct situations such as flying, running or landing) or even just an expression of the phylogenetic history of animals. In the mammalian lineage, it seems improbable that large FCL fossae might be related to bipedalism, because large bipedal primates do not present a fossa while quadruped prosimians do. It is possible that the growth of certain parts of the brain cause the FCLs to expand laterally, not because of an increase in floccular mass but as a consequence of spatial constraints. This leads to the hypothesis that phylogenetic constraint of braincase architecture may play a role in FCL fossa size variation, as is discussed ahead.

Hypothesis III: Locomotion *vs*. FCL size

For locomotor type categories, there are no FCL size patterns associated to different categories. Although hypotheses II and III may look similar, locomotor type categorization allows for a distinction between, for instance, equally agile semi-aquatic and arboreal animals. The data set lacks fossorial animals and this group is worth further study since a relationship between gaze stabilization and FCL fossa size is difficult to support (see "General considerations").

Hypothesis IV: Feeding *vs*. FCL size

Concerning feeding, there are no differences between gatherers, occasional predators and predators when phylogeny is taken into account. Hence, FCL relative size is not capable to unveil details of mammal behavioral adaptations to explore distinct resources. However, there are specializations within each category. For instance, within the predator category, we can find animals with distinct habits and hunting strategies (e.g., ambush, pursuit, semifossorial). With an increased and phylogenetically more restricted data set, it would be possible to outwit the effect of more specific behaviors within general categories (as are predator, gatherer…) in FCL fossa size, as this may be a reason why we could not detect any difference between groups.

Hypothesis V: Optic lobes size *vs*. FCL size

Not tested because mammal brains do not present such structure in their external morphology.

Hypothesis VI: Circadian activity pattern *vs*. FCL size

Although diurnal specimens have on average larger relative FCL size, a phylogenetic analysis of variance detects no difference between diurnal, diurnal/nocturnal and nocturnal animals. Note that on the three categories, the FCL relative size variability is high. This result is not totally unexpected because it is known that many mammals can actually see at night, thus vision is as important as in diurnal species. FCL size variation may be better explained by historical contingencies than by any adaptive pressure to a specific diurnal/nocturnal environment.

Hypothesis VII: Anterior SCC dimensions *vs*. FCL size

The statistical analysis revealed no significant correlation between FCL relative size and ASC relative area. There is, however, a positive trend which is observable in Figure 3.7. I believe this result is not conclusive due to the reduced number of skulls from which ASC area data could be extracted from and, therefore, a braincase architecture constraint should not be discarded. In future work, it would be interesting to increase sample size. The result was similar when relative area was changed by perimeter. This was expected due to the correlation between both these variables.

In general, results show no support to a direct relation of ecological and behavioral patterns in mammals with the size of FCL. This makes clear the need for caution when analyzing FCL fossae sizes and its relation with animal habits.

Birds

Hypothesis I: Body mass *vs.* FCL size

The results do not support any correlation of FCL relative size with body mass. Both heavy and light birds, volant or flightless, present a high variability in FCL relative size. Birds descend from primarily flying ancestors (Voogd & Wylie, 2004), so even heavier and apparently less agile birds are also constrain by its evolutionary history and have maintained a relatively large FCL.

Hypothesis II: Agility *vs.* FCL size

Not tested because a previews study (Walsh et al., 2013) addressed this subject.

Hypothesis III: Locomotion *vs*. FCL size

Not tested because a previews study (Walsh et al., 2013) addressed this subject.

Hypothesis IV: Feeding *vs*. FCL size

Unlike mammals, the difference of FCL size between feeding categories is significant in birds. Although the variability is high, predators have relatively larger FCLs than occasional predators and the group with the smallest relative FCL sizes is the gatherer group. This highlights the importance of vision accuracy in animals which heavily rely on their vision to locate, identify and pursue prey. These results support Franzosa (2004) discussion on cerebellar (including FCLs) growth being related to acquisition of predatory habits. The presence of larger FCL in birds may thus indicate an adaptation to a specific ecological feeding niche.

Hypothesis V/Hypothesis VI: Optic lobes size *vs*. FCL size / Circadian activity pattern *vs*. FCL size

Nocturnal birds show significantly smaller FCL relative size than diurnal ones. This may indicate nocturnal birds are not dependent on vision to navigate or identify obstacles. For instance, using auditory cues, barn owls are capable of locating their prey in total darkness (Payne, 1971), making vision and therefore muscular control of the eye position less relevant. However, owls have a large Wulst, which is the putative homologue of the primary visual cortex in mammals (Reiner et al.,

2005). Wulst neurons are dedicated to spatial frequency, orientation, movement direction and binocular disparity (Nieder & Vagner, 2001). Thus, optic lobes alone are not a good proxy to estimate vision capabilities in birds, at least in strigiforms. If we take this into account, a correlation between FCLs and optic lobes size, as observed in theropod dinosaurs (Fransoza, 2004) is extremely hard to be interpreted. In any case, it should be noted that our data set presents a low amount of nocturnal birds, which may bias the results.

Hypothesis VII: Anterior SCC dimensions *vs*. FCL size

Not tested because data was unavailable.

FCL fossae size as result of cranial architecture

FCL size may be the result of anatomical constraints to which the brain is subjected to by the development of the skull. For instance, cetacean brains have a large floccular complex but lack FCL fossae (Bolk, 1906 *in* Paulin, 1993).

In many cases, although the brain floccular complex is present, it is impossible to measure the FCL volume simply because there is no fossa in some taxa. This is especially problematic in fossil taxa because the actual brain morphology rarely fossilizes and usually only skull endocasts can be used as proxies.

The relationship between the cerebellum as a whole and the periotic and prootic bones is key to understand spatial constraints to FCL dimension. The size of the FCL fossa may depend on the orientation, position or even development of these bones, as a consequence of the enlargement of the cerebellar hemispheres (Olson, 1944). The hypothesis that the FCL size is influenced by skull architecture should be addressed in future works. The mediolateral orientation of the prootic/periotic bone may be related to FCL size. Yet, it is not easy to define an angle of inclination of the prootic in relation to braincase floor, because of the complexity of this bone's form. It might be possible to overcome this problem by segmenting the prootics/periotics on both sides of the skull and define a measurement or ratio to compare distances and inclinations in different species.

Concluding remarks

Our data do not support that the FCL size can be a reliable proxy to infer ecology and behavior in mammals. Birds data analyses show that FCL size patterns are related with a more predatory and mainly diurnal lifestyle. Nevertheless, correlation with visual structures of the brain is not significant. Therefore, potential explanations relating the FCL size with ecology and behavior in fossil taxa should be addressed with extreme caution, given the uncertainty surrounding the implications the FCL relative size. The relationship between the semicircular canals and the FCL and the position of the periotic bones in mammals may represent anatomical constraints that may better explain FCL size variability. There may be correlations involving these spatial constraints provided an increased data

set. Additionally, the homogeneity of the sample can be improved to allow different ecological groups to be equally represented, especially nocturnal birds and fossorial mammals. It would be important to test our hypotheses in more restricted taxonomic groups, as the sample would be more representative of the actual biodiversity. This type of approach to paleoneuroanatomy studies using endocasts must be taken as a case study, because causal relationships must not be assumed before correlations are tested.

References

Agnarsson, I., Zambrana-Torrelio, C. M., Flores-Saldana, N. P., & May-Collado, L. J. (2011). A time-calibrated species-level phylogeny of bats (Chiroptera, Mammalia). PLoS currents, 3.

Akaike, H. (1974). A new look at the statistical model identification. Automatic Control, IEEE Transactions on, 19(6), 716-723.

Albert, J. S. (2001). Species diversity and phylogenetic systematics of American knifefishes (Gymnotiformes, Teleostei) (Vol. 190). Division of Ichthyology, Museum of Zoology, University of Michigan.

Angelaki, D. E., & Hess, B. J. (1994). Inertial representation of angular motion in the vestibular system of rhesus monkeys. I. Vestibuloocular reflex. Journal of neurophysiology, 71(3), 1222-1249.

Balanoff, A. M., Bever, G. S., Colbert, M. W., Clarke, J. A., Field, D. J., Gignac, P. M., ... & Witmer, L. M. (2015). Best practices for digitally constructing endocranial casts: examples from birds and their dinosaurian relatives. Journal of Anatomy.

Blanga-Kanfi, S., Miranda, H., Penn, O., Pupko, T., DeBry, R. W., & Huchon, D. (2009). Rodent phylogeny revised: analysis of six nuclear genes from all major rodent clades. BMC Evolutionary Biology, 9(1), 71.

Burdess, C. (1996). The vestibulo-ocular reflex: computation in the cerebellar flocculus (Doctoral dissertation, Ph. D. thesis, University of Edinburgh).

Butler. M. A.. Schoener. T. W.. & Losos. J. B. (2000). The relationship between sexual size dimorphism and habitat use in Greater Antillean Anolis lizards. Evolution. 54(1). 259-272.

Castanhinha, R., Araújo, R., Júnior, L. C., Angielczyk, K. D., Martins, G. G., Martins, R. M., Chaouiya, C., Beckmann, F. & Wilde, F. (2013). Bringing dicynodonts back to life: paleobiology and anatomy of a new emydopoid genus from the Upper Permian of Mozambique. PloS one, 8(12), e80974.

Christensson, M. (2007). Ontogenetic and comparative aspects of cerebellar and motor development (Doctoral dissertation, Department of Neuroscience, Erasmus Medical Center).

De Zeeuw, C. I., Wylie, D. R., DiGiorgi, P. L., & Simpson, J. I. (1994). Projections of individual Purkinje cells of identified zones in the flocculus to the vestibular and cerebellar nuclei in the rabbit. Journal of Comparative Neurology, 349(3), 428-447.

Domínguez P, Milner AC, Ketcham RA, Cookson MJ, Rowe TB (2004) The avian nature of the brain and inner ear of Archaeopteryx. Nature 430: 666–669.

Faraway, J. J. (2002). Practical regression and ANOVA using R.

Felisa A. Smith, S. Kathleen Lyons, S. K. Morgan Ernest, Kate E. Jones, Dawn M. Kaufman, Tamar Dayan, Pablo A. Marquet, James H. Brown, and John P. Haskell. 2003. Body mass of late Quaternary mammals. Ecology 84:3403.

Fotos, J., Olson, R., & Kanekar, S. (2011). Embryology of the brain and molecular genetics of central nervous system malformation. In Seminars in Ultrasound, CT and MRI (Vol. 32, No. 3, pp. 159-166). WB Saunders.

Franzosa, J. W. (2004). Evolution of the brain in Theropoda (Dinosauria).

Fuchs, A. F., Robinson, F. R., & Straube, A. (1994). Participation of the caudal fastigial nucleus in smooth-pursuit eye movements. I. Neuronal activity. Journal of Neurophysiology, 72(6), 2714-2728.

Gannon, P. J., Eden, A. R., & Laitman, J. T. (1988). The subarcuate fossa and cerebellum of extant primates: Comparative study of a skull-brain interface. American journal of physical anthropology, 77(2), 143-164.

Garland. T.. Jr.. A. W. Dickerman. C. M. Janis. and J. A. Jones. 1993. Phylogenetic analysis of covariance by computer simulation. Systematic Biology 42:265-292

Garland, T. Jr, Ives, A.R. (2000) Using the past to predict the present: confidence intervals for regression equations in phylogenetic comparative methods. Am Nat 155: 346–364.

Gartner, G. E., Hicks, J. W., Manzani, P. R., Andrade, D. V., Abe, A. S., Wang, T., Secor, S.M. & Garland Jr, T. (2010). Phylogeny, ecology, and heart position in snakes. Physiological and biochemical zoology, 83(1), 43-54.

Gilbert, S. F. (2000). Developmental Biology. Sinauer Associates, Inc., Sunderland, MA.

Grafen A. (1989). The phylogenetic regression. Philosophical Transactions of the Royal Society of London. Series B. Biological Sciences 326: 119–157.

Greene, W. H., 2003, Econometric Analysis, 5th ed., Prentice Hall

Hallonet, M. E., Teillet, M. A., & Le Douarin, N. M. (1990). A new approach to the development of the cerebellum provided by the quail-chick marker system. Development, 108(1), 19-31.

Hopson, J. A. (1979). Paleoneurology. Biology of the Reptilia, 9, 39-146.

Hopson, J. A. (1980). Relative brain size in dinosaurs: implications for dinosaurian endothermy. A Cold Look at the Warm-Blooded Dinosaurs. Westview Press Inc., Boulder, Colorado, 287-310.

Ito M (1998) Cerebellar learning in the vestibulo-ocular reflex. Trends Cog Sci 2: 313–321.

Ito, M. (1982). Cerebellar control of the vestibulo-ocular reflex--around the flocculus hypothesis. Annual review of neuroscience, 5(1), 275-297.

Ivakhnenko, M. F. (2008). Cranial morphology and evolution of Permian Dinomorpha (Eotherapsida) of eastern Europe. Paleontological Journal, 42(9), 859-995.

Iwaniuk AN, Nelson J (2002) Can endocranial volume be used as an estimate of brain size in birds? Can J Zool 80: 16–23.

Jerison, H. J. 1973. Evolution of the Brain and Intelligence. Academic Press Inc., New York, New York, 482 pp.

Kheradmand, A., & Zee, D. S. (2011). Cerebellum and ocular motor control. Frontiers in neurology, 2.

Kielan-Jaworowska, Z. (1986). Brain evolution in Mesozoic mammals. Rocky Mountain Geology, 24(special paper 3), 21-34.

Kundrát, M. (2007). Avian-like attributes of a virtual brain model of the oviraptorid theropod Conchoraptor gracilis. Naturwissenschaften, 94(6), 499-504.

Läärä, E. (2009). Statistics: reasoning on uncertainty, and the insignificance of testing null. In Annales Zoologici Fennici (Vol. 46, No. 2, pp. 138-157). Finnish Zoological and Botanical Publishing.
Laaß, M. (2015). Virtual reconstruction and description of the cranial endocast of Pristerodon mackayi (Therapsida, Anomodontia). Journal of morphology, 276(9), 1089-1099.

Larsell, O. (1967). The Comparative Anatomy and Histology of the Cerebellum, from Myxinoids Through Birds: By Olof Larsell. Ed. by Jan Jansen. University of Minnesota Press.

Lavin, S.R., Karasov, W.H., Ives, A.R., Middleton, K.M., Garland Jr, T. (2008) Morphometrics of the avian small intestine, compared with non-flying mammals: A phylogenetic perspective. Phys Biochem Zool 81: 526–550.

Liu, J., Rubidge, B., & Li, J. (2009). A new specimen of Biseridens qilianicus indicates its phylogenetic position as the most basal anomodont. Proceedings of the Royal Society of London B: Biological Sciences, rspb20090883.

Macrini, T. E., De Muizon, C., Cifelli, R. L., & Rowe, T. (2007). Digital cranial endocast of Pucadelphys andinus, a Paleocene metatherian. Journal of Vertebrate Paleontology, 27(1), 99-107.

Maddison WP, Maddison DR (2009) Mesquite: a modular system for evolutionary analysis. Version 2.6. Available: http://mesquiteproject.org.

Martins E. P. & Hansen T. F. (1997). Phylogenies and the comparative method: a general approach to incorporating phylogenetic information into the analysis of interspecific data. American Naturalist 149: 646–667. Erratum vol. 153, p. 488.

McDonald, J. H. (2014). Handbook of biological statistics, 3rd Ed. Sparky House Publishing. Baltimore, MD.

Milner AC, Walsh SA (2009) Avian brain evolution: new data from Palaeogene birds (Lower Eocene) from England. Zool J Linn Soc 155: 198–219.

Miyashita, T., Arbour, V. M., Witmer, L. M., & Currie, P. J. (2011). The internal cranial morphology of an armoured dinosaur Euoplocephalus corroborated by X-ray computed tomographic reconstruction. Journal of anatomy, 219(6), 661-675.

Mundry, R. (2014). Statistical issues and assumptions of phylogenetic generalized least squares. In Modern phylogenetic comparative methods and their application in evolutionary biology (pp. 131-153). Springer Berlin Heidelberg.

Nagao, S. (1992). Different roles of flocculus and ventral paraflocculus for oculomotor control in the primate. Neuroreport, 3(1), 13-16.

Nagao, S., Kitamura, T., Nakamura, N., Hiramatsu, T., & Yamada, J. (1997). Differences of the primate flocculus and ventral paraflocculus in the mossy and climbing fiber input organization. Journal of Comparative Neurology, 382(4), 480-498.

Netter, F. H., Craig, J. A., Perkins, J., Hansen, J. T., & Koeppen, B. M. (2002). Atlas of neuroanatomy and neurophysiology. Icon Custom Communications, Teterboro.

Nieder, A., & Wagner, H. (2001). Encoding of both vertical and horizontal disparity in random-dot stereograms by Wulst neurons of awake barn owls. Visual neuroscience, 18(04), 541-547.

Nyakatura, K., & Bininda-Emonds, O. R. (2012). Updating the evolutionary history of Carnivora (Mammalia): a new species-level supertree complete with divergence time estimates. BMC biology, 10(1), 12.

Olson, E. C. (1944). Origin of mammals based upon cranial morphology of the therapsid suborders. Geological Society of America Special Papers, 55, 1-130.

Pagel, M. (1999). Inferring the historical patterns of biological evolution. Nature,401(6756), 877-884.

Paradis, E. (2011). Analysis of Phylogenetics and Evolution with R. Springer Science & Business Media.

Paulin, M. G. (1993). The role of the cerebellum in motor control and perception. Brain Behavior and Evolution, 41, 39-39.

Paulina Carabajal, A., Lee, Y., Jacobs, L., Kobayashi, Y., Currie, P. (2014). Comparison Of The Endocranial Morphology Of The Nodosaurid *Pawpawsaurus* And Ankylosaurids From North America And Mongolia, With Comments On The Presence Of The Flocculus In The Brain Of Non-Theropod Dinosaurs. Journal of Vertebrate Paleontology, Program and Abstracts, 2014, p.202.

Payne, R. S. (1971). Acoustic location of prey by barn owls (Tyto alba). Journal of Experimental Biology, 54(3), 535-573.

Pearson, R. 1972. The Avian Brain. Academic Press Inc., New York, New

Perelman, P., Johnson, W. E., Roos, C., Seuánez, H. N., Horvath, J. E., Moreira, M. A., Kessing, B., Pontius, J., Roelke, M., Rumpler, Y., Schneider, M. P., Silva, A., O'Brien, S. J. & Pecon-Slattery, J. (2011). A molecular phylogeny of living primates. PLoS genetics, 7(3), e1001342.

Pose-Méndez, S. (2013). Developmental study of the cerebellum of cartilaginous fishes: Towards the identification of primitive features of cerebellar formation in gnathostomes. (Doctoral thesis, Departamento de Biología Celular y Ecología, Facultad de Biología, Universidad de Santiago de Compostela).

Rambold, H., Churchland, A., Selig, Y., Jasmin, L., & Lisberger, S. G. (2002). Partial ablations of the flocculus and ventral paraflocculus in monkeys cause linked deficits in smooth pursuit eye movements and adaptive modification of the VOR. Journal of neurophysiology, 87(2), 912-924.

Reiner, A., Yamamoto, K., & Karten, H. J. (2005). Organization and evolution of the avian forebrain. The Anatomical Record Part A: Discoveries in Molecular, Cellular, and Evolutionary Biology, 287(1), 1080-1102.

Roth, G., & Dicke, U. (2005). Evolution of the brain and intelligence. Trends in cognitive sciences, 9(5), 250-257.

Russell, D. A. 1969. A new specimen of Stenonychosaurus from the Oldman Formation (Cretaceous) of Alberta. Canadian Journal of Earth Sciences 6:595-612.

Schindelin, J.; Arganda-Carreras, I. & Frise, E. et al. (2012), "Fiji: an open-source platform for biological-image analysis", Nature methods 9(7): 676-682.

Sereno, P. C., Wilson, J. A., Witmer, L. M., Whitlock, J. A., Maga, A., Ide, O., & Rowe, T. A. (2007). Structural extremes in a Cretaceous dinosaur. PLoS One, 2(11), e1230.

Shekdar, K. (2011). Posterior fossa malformations. In Seminars in Ultrasound, CT and MRI (Vol. 32, No. 3, pp. 228-241). WB Saunders.

Spoor, F., & Leakey, M. (1996). Absence of the subarcuate fossa in cercopithecids. Journal of human evolution, 31(6), 569-575.

Spoor, F., Garland, T., Krovitz, G., Ryan, T. M., Silcox, M. T., & Walker, A. (2007). The primate semicircular canal system and locomotion. Proceedings of the National Academy of Sciences, 104(26), 10808-10812.

Steppan, S. J., Storz, B. L., & Hoffmann, R. S. (2004). Nuclear DNA phylogeny of the squirrels (Mammalia: Rodentia) and the evolution of arboreality from c-myc and RAG1. Molecular phylogenetics and evolution, 30(3), 703-719.

Takagi, M., Zee, D. S., & Tamargo, R. J. (2000). Effects of lesions of the oculomotor cerebellar vermis on eye movements in primate: smooth pursuit. Journal of Neurophysiology, 83(4), 2047-2062.

Thomas, D. A. (2012). The cranial anatomy of Tenontosaurus tilletti Ostrom, 1970 (Dinosauria, Ornithopoda). Palaeontologia Electronica, 18(2), 1.

Tuyttens, F. A. M., de Graaf, S., Heerkens, J. L., Jacobs, L., Nalon, E., Ott, S., Stadig, L., Van Laer, E. & Ampe, B. (2014). Observer bias in animal behaviour research: can we believe what we score, if we score what we believe?. Animal Behaviour, 90, 273-280.

Van Valkenburgh, B. (1985). Locomotor diversity within past and present guilds of large predatory mammals. Paleobiology, 406-428.

Verzani, J. (2014). Using R for introductory statistics. CRC Press.

Voogd, J., & Glickstein, M. (1998). The anatomy of the cerebellum. Trends in cognitive sciences, 2(9), 307-313.

Voogd, J., & Wylie, D. R. (2004). Functional and anatomical organization of floccular zones: a preserved feature in vertebrates. Journal of Comparative Neurology, 470(2), 107-112.

Waespe, W., Cohen, B., & Raphan, T. (1983). Role of the flocculus and paraflocculus in optokinetic nystagmus and visual-vestibular interactions: effects of lesions. Experimental Brain Research, 50(1), 9-33.

Walker, M. F., Tian, J., Shan, X., Tamargo, R. J., Ying, H., & Zee, D. S. (2010). The cerebellar nodulus/uvula integrates otolith signals for the translational vestibulo-ocular reflex. PLoS One, 5(11), e13981.

Walker, M. F., Tian, J., Shan, X., Tamargo, R. J., Ying, H., & Zee, D. S. (2008). Lesions of the cerebellar nodulus and uvula impair downward pursuit. Journal of neurophysiology, 100(4), 1813-1823.

Walsh S. A., Milner A. C. (2011) Evolution of the avian brain and senses. In: Dyke G., Kaiser G., editors. Living dinosaurs: the evolutionary history of modern birds. Chichester: John Wiley & Sons. 282–305.

Walsh, S. A., Iwaniuk, A. N., Knoll, M. A., Bourdon, E., Barrett, P. M., Milner, A. C., Nudds, R. L., Abel, R. L. & Sterpaio, P. D. (2013). Avian cerebellar floccular fossa size is not a proxy for flying ability in birds. PloS one, 8(6), e67176.

Wilk, M. B., & Gnanadesikan, R. (1968). Probability plotting methods for the analysis for the analysis of data. Biometrika, 55(1), 1-17.
Winship IR, Wylie DRW. 2003. Zonal organization of the vestibulocerebellum in pigeons (Columba livia): I. Climbing fibre input to the flocculus. J Comp Neurol 456:127–139.

Witmer, L. M., Chatterjee, S., Franzosa, J., & Rowe, T. (2003). Neuroanatomy of flying reptiles and implications for flight, posture and behaviour. Nature, 425(6961), 950-953.
York, 658 pp.

Wylie, D. R., De Zeeuw, C. I., DiGiorgi, P. L., & Simpson, J. I. (1994). Projections of individual Purkinje cells of identified zones in the ventral nodulus to the vestibular and cerebellar nuclei in the rabbit. Journal of Comparative Neurology, 349(3), 448-463.

Zee, D. S., Yamazaki, A., Butler, P. H., & Gucer, G. (1981). Effects of ablation of flocculus and paraflocculus of eye movements in primate. Journal of Neurophysiology, 46(4), 878-899.

Ziehen, T. (1899). Makroskopische und mikroskopische Anatomie des Ruckenmarks. von Bardeleben. Handb. Anat. Menwch. 4, Abt. 1-3.

Zuur, A. F., Ieno, E. N., & Elphick, C. S. (2010). A protocol for data exploration to avoid common statistical problems. Methods in Ecology and Evolution, 1(1), 3-14.

Appendix I

This appendix contains images of mammal specimens which were scanned at the HZB or downloaded from KUPRI data base to build this data set. All the specimens are oriented postero-anteriorly (from left to right) and have a 1 cm scale immediately below.

Species list and phylopic.org silhouettes credits

1 – *Allouatta caraya* – Yan Wong

2 – *Anomalurus derbianus* – uncredited

3 – *Arvicola terrestris* – Madeleine Price Ball

4 – *Brachyteles arachnoides* – uncredited

5 – *Cebus apella* – Sarah Werning

6 – *Desmodus rotundus* – Yan Wong

7 – *Dphylla eaudata* – Yan Wong

8 – *Dipodomys deserti* – uncredited

9 – *Felis catus* – David Orr

10 – *Hylobates agilis* – uncredited

11 – *Idiurus macrotis* – uncredited

12 – *Lagothrix lagotricha* – uncredited

13 – *Lepus capensis* – Jan A. Venter, H. T. Prins, David A. Balfour & Rob Slotow

14 – *Lutra lutra* – uncredited

15 – *Marmota marmota* – T. Michaels Keesay

16 – *Meles meles* – uncredited

17 – *Microcebus murinus* – Marky, Gabriella Skollar & Rebecca Lewis

18 – *Molossus rufus* – Yan Wong

19 – *Mus musculus* – David Liao

20 – *Ondatra zibethicus* – Steven Traver

21 – *Oryzorictes* sp. – Mo Hassan

22 – *Otolemur crassicaudatus* – Josaph Wolf & Dinah Challen

23 – *Paradoxurus* sp. – Pearson Scott Foresman

24 – *Petaurus* sp. – Sarah Werning

25 – *Potamogale velox* – Mo Hassan

26 – *Presbytis melalophus* – Yan Wong & Joseph Smith

27 – *Prionailurus iriomotensis* – Steven Traver

28 – *Procavia capensis* – Steven Traver

29 – *Propithecus verreauxi* - Terpsichores

30 – *Pteropus* sp. – Oron Peles & Yan Wong

31 – *Puma concolor* - Lukasiniho

32 – *Rattus norvegicus* – Rebecca Groom

33 – *Ratufa affinis* – Catherine Yasuda

34 – *Ratufa bicolor* – Catherine Yasuda

35 – *Rhinolophus ferrumequinum* – Yan Wong

36 – *Rousettus aegyptiacus* – Steven Traver

37 – *Sciurus vulgaris* – Catherina Yasuda

38 – *Talpa europaea* – Steven Traver

39 – *Ursus americanus* – Tracy A. Heath

40 – *Varecia variegata* – Yan Wong

41 – *Vulpes vulpes* – Rebecca Groom

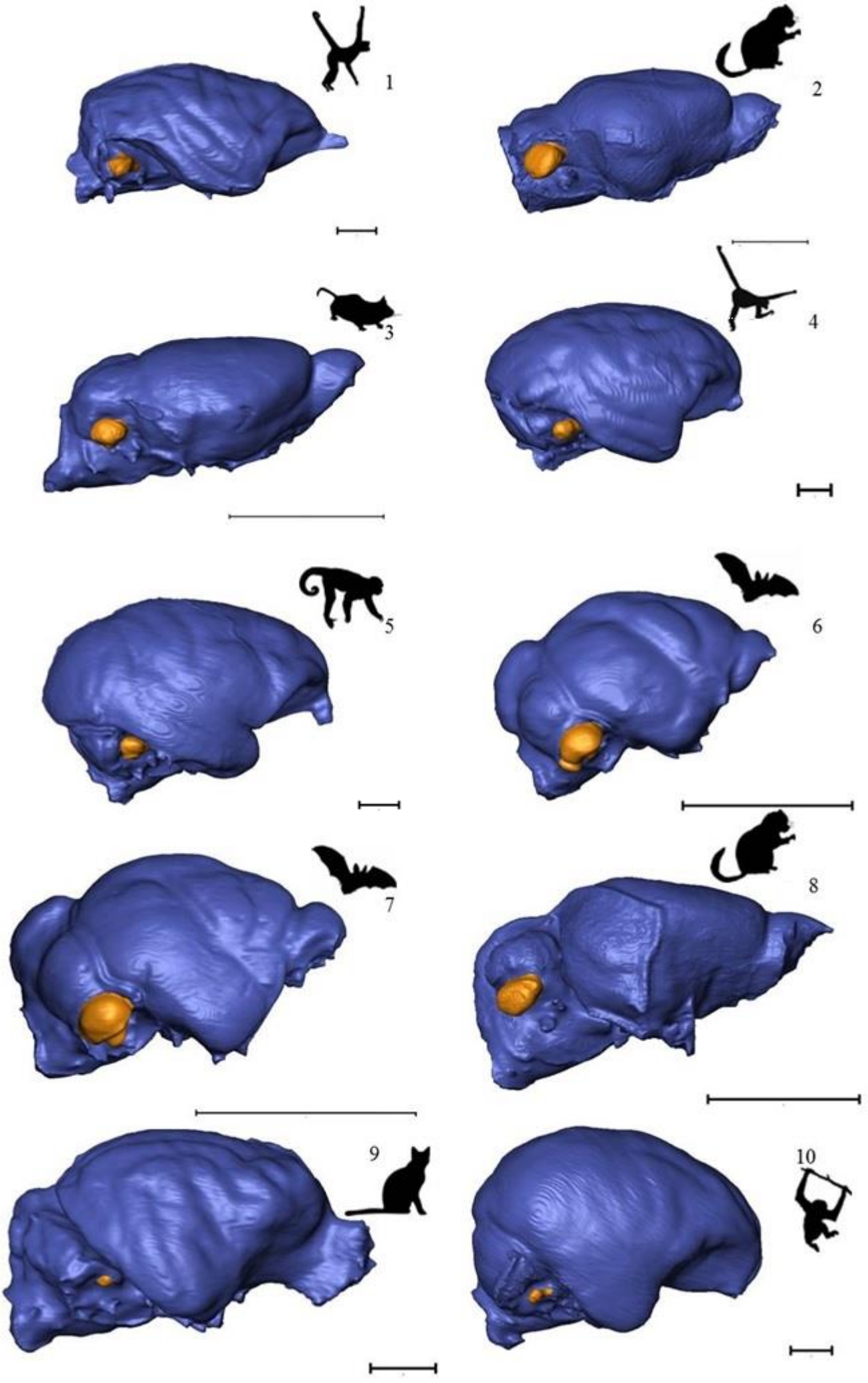
1
2
3
4
5
6
7
8
9
10

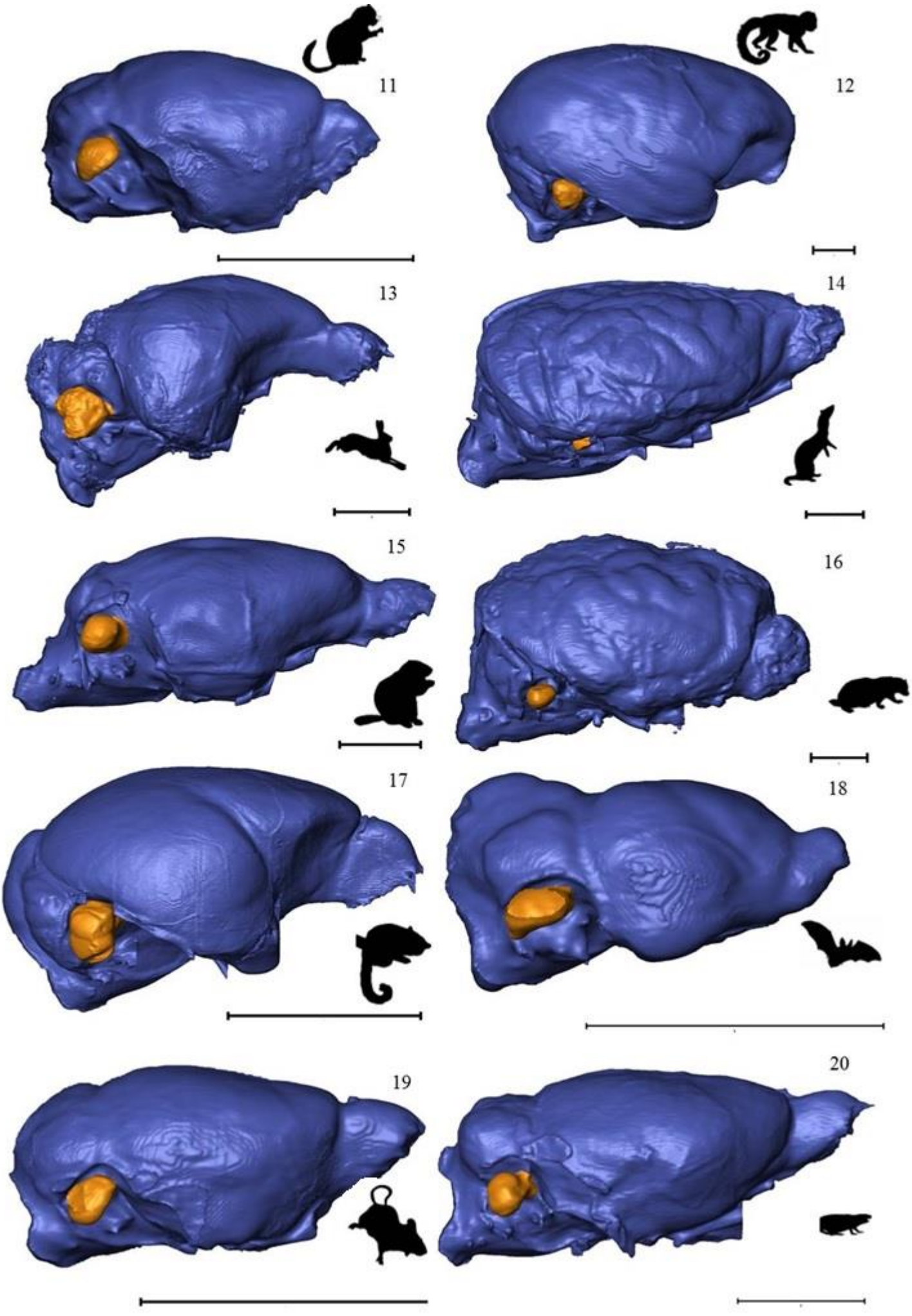
11
12
13
14
15
16
17
18
19
20

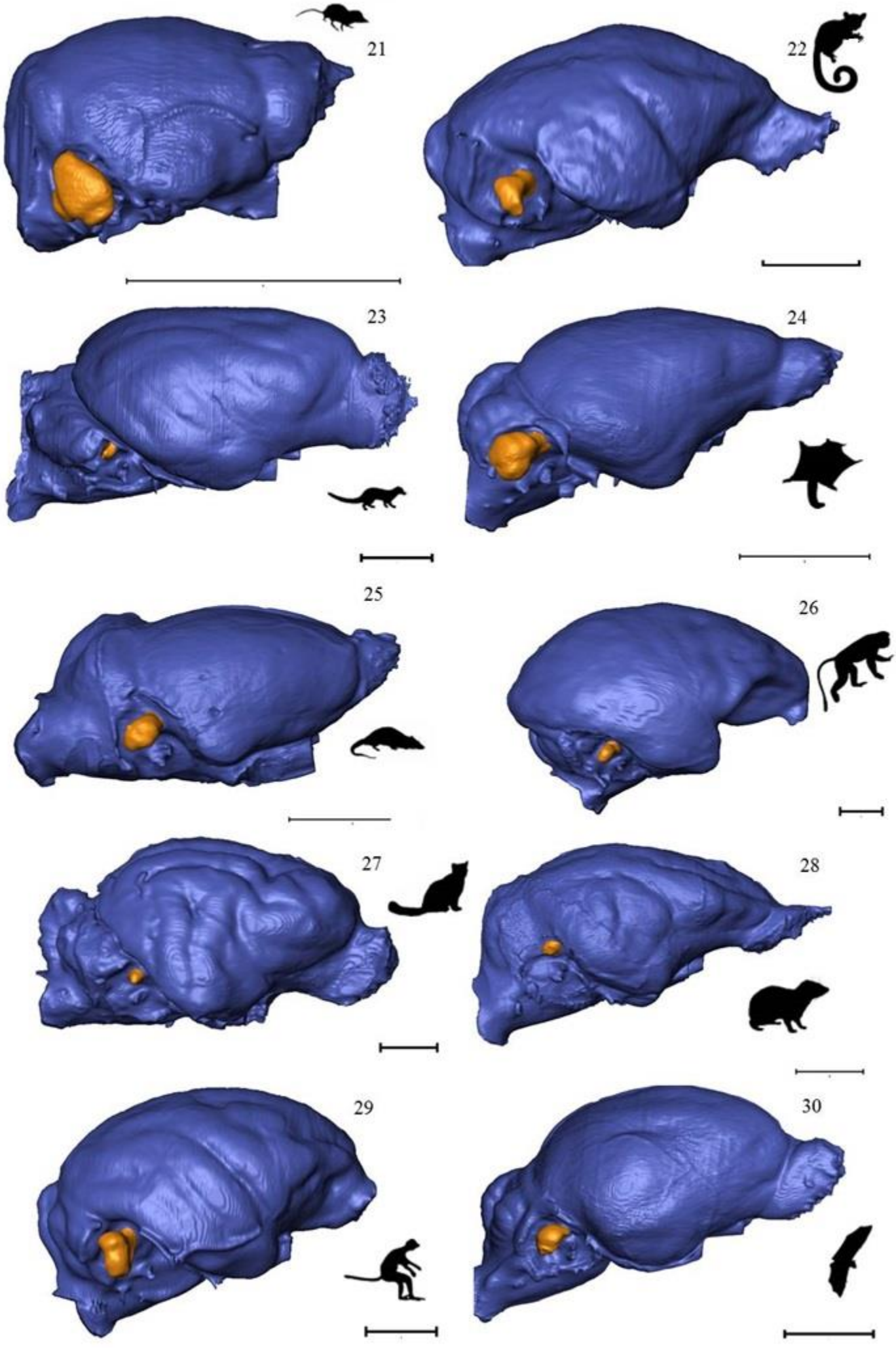
21
22
23
24
25
26
27
28
29
30

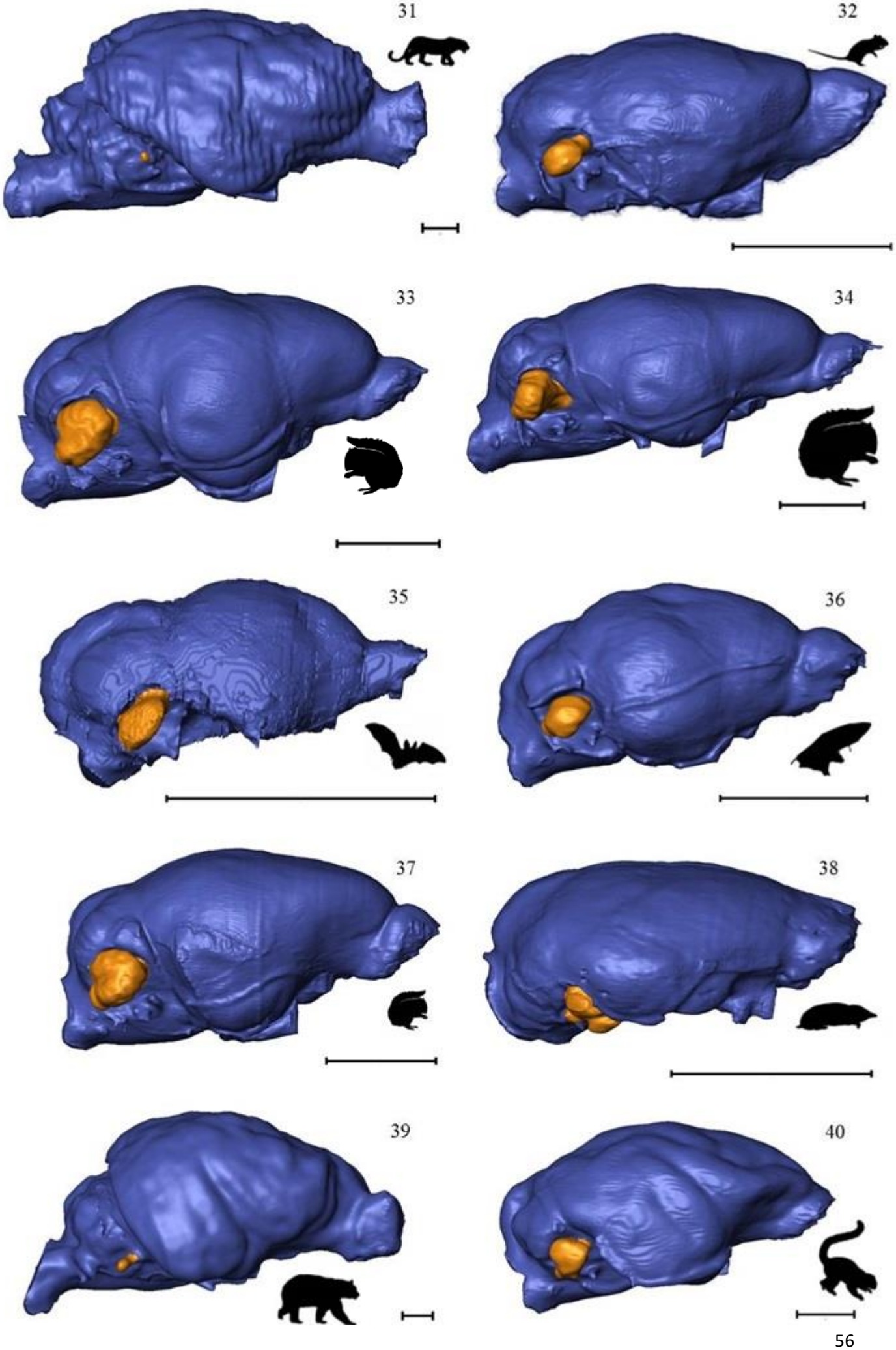
31
32
33
34
35
36
37
38
39
40

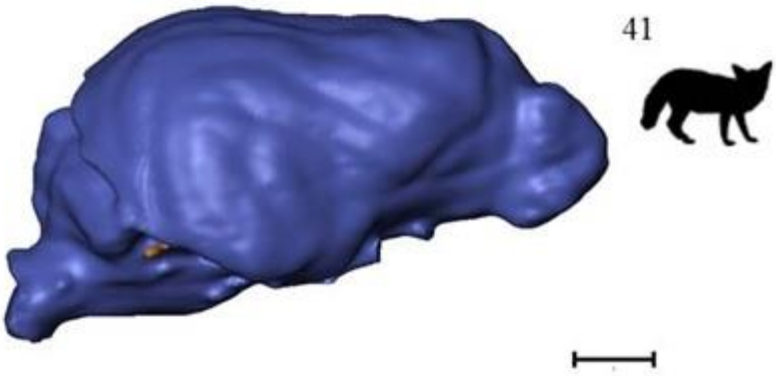
41

Appendix II

In this section I present two peer-reviewed abstracts accepted for oral communications at the Society of Vertebrate Paleontology Annual Meetings in 2014 and 2015.

- **Ferreira-Cardoso, S., Araújo, R., Castanhinha, R., Walsh, S., Martins, R.M.S., Martins, G.G. (2014). The Floccular Complex: neuroanatomy as a tool to unveil paleoecology. Journal of Vertebrate Paleontology, Program and Abstracts, 2014, p.128. – SVP 2014 Berlin, Germany.**

Comparative neuroanatomy in vertebrate evolution provides deep insights into how brain structures evolved through time, their functions and relative importance. A central principle in neuroanatomy is that there is a relation between relative neural tissue volume and its functional importance. The floccular complex of the cerebellum, formed by the flocculus and the ventral paraflocculus (housed in the floccular fossa), integrates visual and vestibular information and is responsible for the vestibulo-ocular reflex, smooth pursuit and gaze holding (movements of the eye to fix an object in motion). The ubiquity and universal function of this complex led us to hypothesize that the floccular complex relative volume might be a proxy to infer animals’ ecology. Some authors referred to variations of the floccular complex volume and its relation with body mass with putative increased vision capacity and body agility. However, no comprehensive study has yet been performed in order to address this issue.

We analyzed brain cavity endocasts from diverse extinct and extant taxa to assess the relationship between the floccular complex volume and ecological variables. We tested the following hypotheses: 1) there is a correlation between optic lobes and floccular complex volume; 2) there is a negative allometry relation between the floccular complex volume and body mass; 3) floccular complex volume varies according to locomotion type and feeding habits. We integrated data from distinct taxa and associate floccular complex size patterns with specific ecological niches. The emydopoid dicynodont Niassodon mfumukasi is an interesting outlier given that the floccular complex relative volume to its brain volume is unexpectedly large. This ratio is 1,9%, comparable to that of some passerine birds well known for their agility (e.g. swallows), which might indicate that a direct relationship between floccular size and behavior is far from being well understood.

- **Ferreira-Cardoso, S., Castanhinha, R., Araújo, R., Walsh, S., Martins, N.E.V., Martins, R.M.S., Martins, G.G., Kardjilov, N., Hilger, A. (2015). Floccular Complex Lobe size does not correlate with vertebrate ecology and behavior. Journal of Vertebrate Paleontology, Program and Abstracts, 2015, p.123. – SVP 2015 Dallas, Texas.**

The floccular complex lobes (FCL), housed in the FCL fossa of the prootic and periotic, are part of the cerebellum. Several experimental studies have shown that the FCL integrate visual and vestibular information, responsible for the vestibulo-ocular reflex, smooth pursuit and gaze holding. Thus, over the last decades multiple paleoneurological studies have been extrapolating these results to infer a causal relation between FCL size and behavior of extinct forms.

We analyzed braincase endocasts of a representative sample of Mammalia (48 species) and Aves (60 species) rendered using tomographic segmentation techniques. We tested statistical correlations between the floccular complex volume, ecology and behavior that could support previous paleobiological assumptions. The data was analysed using three models of trait evolution and covariance structures (Pagel's Lambda Model, Brownian Motion Model and Grafen's Rho Model) to produce phylogenetic generalized least-squares regressions. Phylogenic trees were built and all branch lengths were set to one. Our results convincingly demonstrate that: 1) there is no correlation between

relative FCL volume and body mass; 2) there is no correlation between relative FCL and optic lobes size in birds; 3) average relative FCL size is larger in diurnal than in nocturnal birds but there is no statistically significant difference in mammals; 4) feeding strategies do not correlate with FCL size; 5) locomotion type is not correlated with relative FCL size in mammals.

We conclude that the cerebellum is a highly plastic structure and may be adapted to control different functions across different taxonomic levels. For example, the european mole (Talpa europaea) which is fossorial and practically blind, has a FCL fossae relative size larger than those of bats, which are highly maneuverable, and comparable to the value of African gliding rodents (Anomaluridae) or the flying phalanger (Petaurus sp.). Therefore, until further experiments are done, we recommend that ecological and behavioral traits of extinct animals should not be inferred based on FCL fossae relative size. Alternatively, we here suggest that the evolution of the FCL fossae relative size variations might be better explained by factors such as anatomical trade-offs or other developmental constraints. It has not escaped our notice that further research is needed to challenge several other paleoneurological hypotheses that are simultaneously widely accepted and narrowly tested.